## Making flying microgrids work in future aircrafts and aerospace vehicles

Marija D. Ilić<sup>a</sup>, Rupamathi Jaddivada<sup>a</sup>

<sup>a</sup>Massachusetts Institute of Technology, 77 Massachusetts Avenue, Cambridge, 02139, MA, USA

#### **Abstract**

This paper concerns modeling, simulations and control design of turbo-electric distributed propulsion (TeDP) systems needed to power future hybrid aircraft systems. The approach taken is the one of control co-design by which the sizing and hardware selection of components and the TeDP architecture design are pursued so that potential effects of control and automation are accounted for from the very beginning. Unique to this approach is a multi-layered modular modeling and control approach in which technology-specific modules comprising the complex dynamical system are characterized using unified interaction variables at their interfaces with the rest of the system. The dynamical performance of the interconnected system is assessed using these technology-agnostic interface variable specifications and, as such, can be applied to any candidate architecture of interest. Importantly, even the inputs to the TeDP system coming from pilot commands are modeled using such interface variables. This new multi-layered modeling captures the dynamics of energy and power as interactions. It also has a rather straightforward physical interpretation. The paper builds on our earlier results introduced for terrestrial power systems, including small micro-grids. We show how system feasibility and stability can be checked in real-time operations by modules exchanging the information about their interaction variables and adjusting in a near-autonomous manner so that, as system conditions vary, the interconnected system still functions. No such systematic control co-design exists to the best of our knowledge, but it is needed as both new technologies and more complex, often conflicting performance objectives emerge. We illustrate the approach on a representative TeDP architecture and compare it to today's state-of-the-art. We close with a discussion on the generalization of the method for any given candidate architecture. Having such an approach dramatically reduces the R&D&D of novel candidate architectures.

*Keywords:* Turbo-electric distributed propulsion (TeDP), Modeling and control of power trains for aircrafts, Microgrids, Interconnected dynamic systems, Distributed Control, Energy and Power Dynamics

## 1. Introduction

This paper introduces a new modeling, simulations and control approach to power trains in complex aircraft and other aerospace space vehicle systems by viewing them as dynamically interacting interconnected modules. These power trains are effectively "flying microgrids" comprising diverse power sources (permanent magnet (PM) machines, DC generators, synchronous machines (SM), doubly-fed induction generators (DFIG) rotating at different speeds) interconnected via AC/DC power electronically-controlled inverters of dispersed storage, such as small batteries and/or capacitors. Such systems have never been modeled to the degree of granularity required to ensure stable and efficient

performance over broad ranges of operating conditions. This is an important problem that is closely related to the composability of heterogeneous dynamical components and their specifications for contributing to the desired performance of the system. This problem has been tackled in the past by practitioners defining the mappings at interfaces based on experimental/expert system knowledge or by the theoreticians establishing conditions hard to relate to the physical processes in the complex system. The two approaches can hardly ever be related and, more importantly, cannot be used for powering challenging future missions. This paper overcomes the static mappings traditionally utilized at the interfaces and, instead, specifies input-output characteristics of components/group of components using dynamical modeling in energy/power state space and, as such, sets the basis for relating the mathematical conditions to the physical processes.

Email addresses: ilic@mit.edu (Marija D. Ilić), rjaddiva@mit.edu (Rupamathi Jaddivada)

In this new modeling approach, each module comprises a group of components in which dynamics of physical variables are modeled first in standard state space form, generally used for control design. Second, the model is transformed into a higher-level general technology agnostic model. This recently proposed transformed state space model represents the dynamics of stored energy and its rate in each of these modules within any power train. The interaction variables, the key to modeling and controlling mutual effects of components are shown to be instantaneous real and instantaneous reactive power. This modeling approach sets the basis for capturing effects of highly different sub-processes, such as the inter-dependence of power electronically controlled components and thermal processes; interdependence across the entire turbo-electric distributed propulsion (TeDP) and alike. For the first time, dynamics of interconnected energy sources (generators) of different types (DC, DFIG, SM) and the propulsor/fans of different types are modeled for provable control design, with a clear understanding of physical processes, such as balancing of power and its rate of change.

The interconnected dynamic model is systematically derived by writing conservation of both real power and rate of change of reactive power. Notably, the notions of instantaneous real and reactive power, typically defined for electric systems, are defined for all types of energy conversion modules the same way by utilizing the effort-flow analogies. These models provide great physical intuition about energy conversion dynamics in these complex systems, as the proposed model in transformed state space has a straightforward interpretation in terms of exergy and anergy. Both efficiency and stability conditions become apparent. Based on these concepts, it becomes possible to understand potential benefits from new technologies. For example, in this paper, several different power train designs for future air vehicles are modeled and their energy-based control is simulated and assessed. A sliding mode control (SMC) robust implementation of this energy-based control is introduced, and theoretical conditions are derived for near-optimal stable control design at provable performance. Future extensions of these concepts to modeling and controlling complex aircraft and other vehicles are discussed.

The paper is organized as follows: In Section 2 the need for hybrid power trains is briefly described. In Section 3 power train design as a control co-design problem for complex dynamical systems is introduced. In Section 4 a multi-layered modeling in transformed energy state space is summarized and illustrated on a simple

TeDP architecture. This is followed in Section 5 by summarizing distributed feasibility and stability conditions in energy space. In Section 6 a control co-design is formulated, and it is shown how it can be implemented so that the feasibility and stability conditions are met. In particular, a general method for designing future power trains for ensuring feasible and stable operations for given ranges of missions and according to given performance objectives is introduced. In Section 7 representative examples of candidate architectures are discussed from the viewpoint of their performance based on today's approaches. Benchmarking is done by assessing whether the proposed approach meets today's equipment testing standards. Notably, the end-to-end system performance standards are not in place. These are created by drawing on comparisons with general Multi-Input Multi-Output (MIMO) Linear Quadratic Regulating (LQR) control combined with state-of-the-art controllers of individual equipment. Finally, in the closing Section 8 summary of the proposed approach is given together with several open questions and ideas for future R&D&D.

#### 2. Motivation

The approach proposed in this paper is motivated by several reasons. First, and perhaps most important, is that the expected performance of future aircraft and other space vehicles is becoming more complex and demanding than in the past. In addition to ensuring safe and reliable power provision to the aircraft, the power train should be able to minimize fuel use and reduce noise and emissions [30]. Today's allmechanical power trains are rigid and hard to design for accommodating new placement of propulsors for more efficient flights [12]. Also, fast missions and sudden unplanned maneuvers require fast control of power management. Candidate TeDP architectures comprising power electronically-controlled secondary generation, storage and motors hold a new promise of enabling safe and flexible power. The required technological advances are being made. The fundamental challenge comes from having to design and control these manmade systems for the first time. The required R&D&D is very challenging given the overall complexity of these emerging architectures.

Technical challenges are multi-fold and come from the need to understand dynamical interactions between highly heterogeneous components and to design their control and protection. Having secondary power sources lead to new operating problems, such as supporting bidirectional power flows when needed. The highly time-varying missions require the control design to produce power at the rate needed to ensure feasibility and stability. Most challenging are emerging operating problems during unplanned equipment failures. Ideally, it would be good to have self-adaptation for safety in an autonomous way and, at the same time, not trigger protection.

## 2.1. Lack of dynamical system approaches

Most of the ongoing efforts are toward better standalone hardware components and materials. At the same time, there are simulation-based approaches to assessing the performance of these candidate architectures. Selection of the best type of electric machines, both generators and motors, and their integration into well-functioning end-to-end TeDP systems for satisfying given flight specifications are currently being done for specific candidate architecture on a case-by-case basis. This design method is time-consuming and does not enable quick screening of several architectures and selecting the one best suited for given flight specifications.

It may come as a surprise that there has been very little work done on systematic modeling for the control of TEDP architectures. The modeling and control of even a small system comprising a permanent magnet (PM) generator expected to rotate at the same speed as the engine and supplying a propulsor motor rotating at a different speed and controlling torque or power given from the pilot command remain an open problem at present. The controllable equipment is currently tested against the static step changes in power outputs so that the transient and steady-state responses following step-change meet certain frequency and voltage specifications [26]. The problem of supplying continuously varying power or torque is qualitatively different, as will be described in the simple voltage-controlled RL circuit in Appendix A [23]. It considers the easiest control design problem in the context of the circuit in Figure A.16 to control voltage u(t) to exactly regulate port voltage v(t). This results in producing of controlled power  $P_u(t)$  to match power seen by the component  $P_m(t)$ . However, due to measurement errors and control implementation delays, there is a power mismatch  $\Delta P(t)$  which could lead to oscillations between the controlled component and the rest of the system, particularly when the component inertia, in this case, inductance L is small. Also, if the power mismatch  $\Delta P(t)$  sustains over time, this could lead to increasing mismatches and protection disconnecting equipment.

This simple example without loss of generality illustrates the need for more coordinated control of interconnected dynamical components. This need brings up

questions regarding the performance of TeDP architectures based on centralized fast communications, on the one hand, and distributed cooperative control, on the other. In this paper, we describe the general complexity of the centralized model and its fail-safe communication needs for provable performance. In turn, these point into the direction of requiring distributed control implementation, which further raises questions regarding the achievable performance in a distributed way. These general questions and challenges have prompted us to introduce a multi-layered control design proposed in this paper.

# 3. TeDP architecture as a complex dynamical system: Problem posing

Possible TeDP designs could be to use different types of electrical machines, mainly either PM or DC machines, or their combinations. More advanced machines, such as doubly-fed induction generators (DFIG) [5], and switched reluctance motors [4] are also being considered for power trains in future aircraft systems. In this paper we consider two such designs shown in Figures 1 and 2, respectively. Also, a typical design

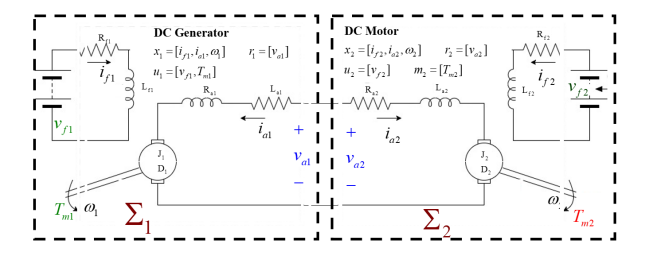


Figure 1: An example TeDP system comprising DC machines

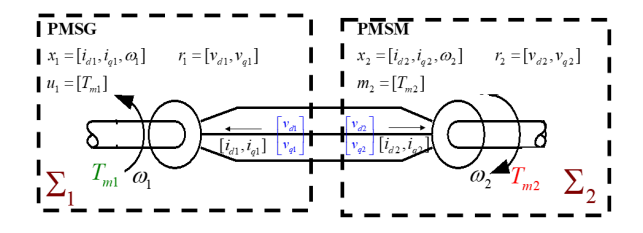


Figure 2: An example TeDP system comprising permanent magnet machines

involves the need for generators and motors to move at different speeds  $\omega_1^{ref}(t)$  and  $\omega_2^{ref}(t)$ , respectively. This, in turn requires some sort of AC/DC and DC/AC conversion [24], or some other novel designs, including resonant converters [29]. Shown in Figure 3 is a sketch

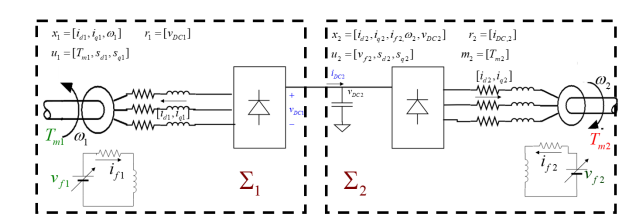


Figure 3: An example TeDP system comprising synchronous machines connected through an AC-DC-AC converter

of such power electronically controlled system. We consider all these systems as interconnected dynamical systems whose interactions and performance are determined by embedded automation and control. Two qualitatively different design problems arise. Most generally,

Figure 4: A general TeDP system comprising sub-systems  $\Sigma_1$  and  $\Sigma_2$  interacting through port inputs  $r_1, r_2$ . The system is subject to a possibly state-dependent time-varying torque disturbance m2 that is expected to be controlled through the available controllable inputs

any of these typical representative TeDP architectures can be conceptualized as shown in Figure 4. The basic functionality of this interconnected system is to produce power or torque by the motor in order for its rotor to move fans. Depending on the design of interest, this can be achieved by controlling the motor as a variable speed drive (VSD) or by directly controlling torque or power absorbed by the rest of the system. For example, when  $\Sigma_2$  in the TeDP system in Fig. 4 powers a fan, the disturbance  $m_2$  is characterized as the torque  $T_{m,2}$  which is generally modeled as

$$T_{m2} = T_{m2,0} \left( \frac{\omega_2}{\omega_{2,0}} \right)^{\epsilon} \tag{1}$$

Here,  $\omega_2$  is the angular frequency of the motor.  $T_{m2,0}$ ,  $\omega_{2,0}$  represent nominal values of the load torque and angular frequency respectively.  $\epsilon$  can take the values of 0, -1 and 2 to model loads of different types called constant torque load, constant power load and a propulsive load, respectively.

When  $\epsilon = -1$  the performance requirement is for motor rotor to follow given instantaneous power. This requirement has been known to be quite challenging because of inherent negative incremental impedance problem for some ranges of power [1]. Shown in Figure 5

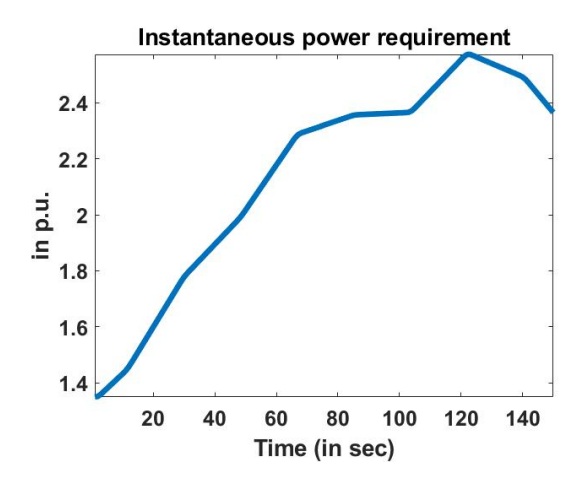


Figure 5: Typical mission requirements: Instantaneous power requirement of the fans driven by the motors

are such typical performance objectives. First, when the mission trajectory is quasi-stationary compared to the system dynamics, it is possible to have a feed-forward (tertiary) level coordinating scheduler of set points for the controllable equipment so that commands are given in a top-down way to regulate and stabilize the controllers so that power is provided in response to the higher level commands. The second design problem is to enable power train to respond to hard-to-predict both relatively slow and fast changes from nominal schedules in an autonomous way without being given feedforward commands. While this distinction seems to be secondary, it is actually quite important for designing stable and feasible control to enable TeDP power over broad ranges of time varying conditions. Today's approach to design and control power train is so that during (N-1) or (N-2) equipment failures known based on experience and off-line simulations studies the objectives are still met. The second design problem is much more challenging because the control and automation must be much more self-adaptive without having predicted conditions.

## 3.1. Nonlinear MIMO control design problem

The machine models in each of the architecture in Fig. 1-3 are reviewed in some detail in Appendix Appendix B. Notably, a closer look into a general electric machine modeling shows that, independent from the type of the machine, its dynamical standard state space model needed for control design takes on the following general form:

$$\dot{x}_i = f_{x,i}(x_i) + g_i^r(x_i)r_i + g_i^m(x_i)m_i + g_i^u(x_i)u_i$$
 (2)

Here,  $x_i$  represents the state variable of the component i. The inputs entering the electric machine are the port inputs, controllable inputs, and exogenous disturbances denoted as  $r_i$ ,  $u_i$  and  $m_i$ , respectively. Not all the components have all the types of inputs entering. For instance, in Figure 4, the disturbances  $m_2$  enter component 2 alone.

A linearized counterpart of Eqn. (2) is then given as

$$\dot{x}_i = A_i(x_i^*, u_i^*) x_i + B_i(x_i^*) \begin{bmatrix} r_i & u_i & m_i \end{bmatrix}^T$$
 (3)

Here,  $x_i^*, u_i^*$  respectively represent the equilibrium state and control for the present value of the port and disturbance inputs  $r_i^*, m_i^*$ , respectively. It is only when switching models are to be utilized such as for the one in Fig. 3 that the component models take the form in Eqn. (3). In general, however, most TeDP architectures have constant matrix  $B_i$  and the matrix  $A_i$  is only state dependent. The interconnected TeDP models are constructed by obtaining expressions for port inputs in terms of the state variables of the neighboring components by applying basic Kirchoff's laws at the junction [3]. However, for the architectures in Fig. 1 and 2, the inherent structure of the machine models in Eqn. (2) is lost due to the presence of dependent states resulting from inductor cutsets [3]. The state of the art approach for analysis of such systems has been to introduce a capacitor between the components such as the one in Fig. 3 to preserve the inherent structure of the stand-alone machine and thereby design the stand-alone control.

As an example for the DC system architecture in Fig. 1, the stand-alone DC generator (motor) torque (armature) and field control are designed using timescale separation-based model reduction [6]. DC machine models are linear except for dependence of the matrix  $A_i$  on field current state. Timescale separation is, therefore, utilized to facilitate decoupled control of field and angular speed (terminal voltage).

Another state of the art approach commonly utilized is the field oriented control first introduced for induction machines [27]. It utilizes a transformed space to facilitate decoupled control of flux and angular speed (or terminal voltage) in a way similar to that of DC machines. Synchronous machines have two degrees of control (field voltage and torque). Often the disturbances are such that the terminal voltage does not change much. In such cases architecture in Fig. 2 with a single degree of control is sufficient. Other times, it is ensured so by introducing a large buffer capacitors between the machines. In the absence of synchronous machines with field control, another alternative is to insert an AC-DC-AC converter to provide additional degree of

control, as sketched in Figure 3.

The stand-alone control designed by assuming the component is disconnected from the rest of the system is not provable from the systems point of view especially in the presence of fast time-varying disturbances. To ensure decoupled control design results in stability, an additional buffer capacitance possibly with power electronics is needed, which adds to the weight of the TeDP system.

Another alternative approach is to design an LQR centralized control from the linearized system model. It should be noted that it is not straightforward to obtain error-free interconnected system models in the absence of buffer capacitor between components. We have utilized a software called CAMPS (Centralized Automated Modeling of Power Systems) that constructs interconnected system models in an automated way [21, 15] and which has been further developed to simulate TeDP architectures [28]. The software also has additional functionalities to find the equilibrium, perform linearized stability analysis and compute the most critical states contributing to instability, and to design LQR tuned gains for the controllers. This LQR control is treated in this paper as the benchmark control.

Although CAMPS does systematic design, the approach is generallly not applicable to designing provable performance control in response to large ranges of disturbances, since the linearized models utilized for control design are provable only for small perturbations around the operating point where tuning is done. For sudden changes in operating conditions, a new nonlinear MIMO control problem has to be formulated, instead.

Notably, independent from the specific structure and internal primary control design problem, we make following observations:

- Generally, the control design problem in standard state space is a nonlinear control problem.
- The interconnected TeDP system becomes a nonlinear MIMO control design problem, for which no general off-shelf designs exist.

When different advanced machine controllers are designed they are tested so that their own output variables of interest (frequency, voltage) meet specifications. Given the discussion in Appendix A, it is not clear how the component will interact with the rest of the system. It is with these observations in mind that we introduce our energy space multi-layered modeling for control design.

# 4. Unified multi-layered modeling of a TeDP using transformed energy state space

The fundamental issues of the emerging TeDP systems are made evident through the simulations of a simple resistive inductor circuit example in Appendix A. In summary, the traditional control approaches are based on models constructed from the first law of energy conservation principles alone. Such models do not consider the rate at which the external power injections  $P^m$  enter. This time-variation could be a result of challenging TeDP mission requirements. However, it can also be because the decentralized control actions are most often taken by each of the components in the TeDP systems. For instance, in the system of Fig. 1,  $P^m(t)$  seen by  $\Sigma_1$ is a result of the inherent dynamics and control actions taken in  $\Sigma_2$ . As a result, its dynamics can not necessarily be counteracted by disturbance rejection-type of control that is synthesized by traditional approaches utilizing static power measurements of  $P^m$ . Furthermore, such an approach does not explicitly consider the rate at which  $P^m$  varies, which may jeopardize the overall system stability.

Aforementioned issues are marginally overcome today in energy systems through over design and conservative control strategies. One example of such conservative control is to prepare the system for the worst possible operating conditions. However, the root cause of non-provable control design is the lack of sufficiently granular models needed to capture the dynamics of interactions between sub-systems. In this paper, we propose a multi-layered modeling in transformed state space to capture interactions from the very beginning to perform control co-design. The model in transformed state space is derived for precisely capturing the dynamics of interactions between sub-systems through a well defined physical quantity in phasor domain in electrical energy systems called reactive power. This physical quantity was defined in time-domain for the first time in [32]. We generalize it for multiple energy domains and use it to develop a sufficiently rich model for analyzing and controlling the dynamics of interactions.

We consider any candidate architecture, partitioned into sub-systems as shown in Fig. 1 - 3. Note that the partitioning is non-unique and it depends very much on the knowledge of state variables needed for distributed control design. We then zoom-in to each of the modules for control design to specifically shape certain variables called interaction variables that have special structural properties. We show that each component needs to satisfy certain feasibility and stability conditions by its interaction variables, upon which it can be integrated with

rest of system. These steps are to be performed through information exchange with neighbors in an interactive manner. These are also the general steps introduced in [10] for control co-design. In this paper, we simplify the task of control co-design by the introduction of unified dynamical models based on interaction variables and making different steps involved in control co-design seamless.

The standard state space models introduced in Eqn. (2) are a result of first law of energy conservation. We have derived unified energy-based models to capture the the rate of change of the energy component that does useful work and wattless work required for energy transfer, referred to as exergy and anergy, respectively. Notably, this model observes both first and second law of thermodynamics. The modeling relies on harnessing the structural properties of an interaction variable, which are defined as follows [16, 19, 23]:

## **Definition 1.** (Interaction Variable) [16, 23] <sup>1</sup>

Let  $E_i$ ,  $p_i$ ,  $P_i^u$ ,  $P_i^m$ ,  $\dot{Q}_i^u$ ,  $\dot{Q}_i^m$  represent the stored energy, rate of change of stored energy, instantaneous power at control terminal and disturbance terminal and generalized rate of reactive power at control and disturbance terminals respectively of component i. Each of these variables is computable as a function of local state variables and state derivatives, summarized in Appendix C.

The interaction variable  $z_i^{r,out}$  is defined as a function of local variables that satisfies the property.

$$z_i^{r,out} = constant$$
 (4a)

when all interconnections are removed. Mathematically, the interaction variable is defined as

$$z_{i}^{r,\text{out}} = \begin{bmatrix} \int_{0}^{t} \left( p_{i}(s) + \frac{E_{i}(s)}{\tau_{i}} - P_{i}^{u}(s) - P_{i}^{m}(s) \right) ds \\ \int_{0}^{t} \left( -\dot{p}_{i}(s) + 4E_{t,i}(s) - \dot{Q}_{i}^{u}(s) - \dot{Q}_{i}^{m}(s) \right) ds \end{bmatrix}$$
(4b)

In order to differentiate the interactions resulting from internal energy conversion processes as per the Definition 1, and the ones obtained as a result of interconnection, we utilize the superscripts 'out' and 'in' respectively. The incoming interaction variable is a result of interconnection, as shown in the zoomed-out representation of the interconnected system in Fig. 6. Notice

<sup>&</sup>lt;sup>1</sup>This definition was provided in particular for electric power systems under an assumption of real-reactive power decoupling [16, 17]. We now further extend this notion by relaxing the decoupling assumption.

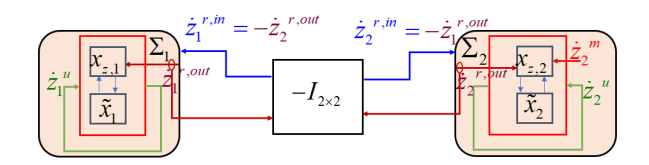


Figure 6: Zoomed-out representation for the interconnected system: Incoming interactions  $(z_i^{r,in})$  are shown with blue arrows, while the outgoing ones  $(z_i^{r,out})$  by virtue of local energy conversion dynamics are shown in brown for each of the components in the closed-loop. After interconnection, the incoming interaction variable is equal to the negative of outgoing interaction variables of its neighbors.

that the outgoing interaction variables as per Definition 1 depend only on local state variables and their derivatives. Its time derivative however depends on the rate of change of the incoming interaction variables  $\dot{z}_i^{r,in}$  that are function of state variables of other components in the system.

## 4.1. Unified energy-based higher-layer model

The interaction variables defined in Eqn. (4b) drive the the dynamics of energy  $E_i$  and its rate of change  $p_i$ , the model of which is provided in Eqn. (5a). Here, the state variables are aggregate dynamical energy variables denoted as  $x_{z,i} = [E_i, p_i]^T$ .

Energy space state dynamics: 
$$x_{z,i}(0) = x_{z,i0}$$
 (5a)  
 $\dot{x}_{z,i} = A_{z,i}x_{z,i} + B_tE_{t,i}(\dot{x}_i) + B_z\left(\dot{z}_i^{r,out} + \dot{z}_i^u + \dot{z}_i^m\right)$   
Rate of change of common outputs:  $z_i^{r,out}(0) = z_{i0}^{r,out}$   
 $\dot{z}_i^{r,out} = \phi_{z,i}(x_i, r_i, u_i, m_i, \dot{z}_i^{r,in})$  (5b)

In this model,  $E_{t,i}$  is the stored energy in tangent space as defined in Definition 5. It models higher-order effects of local state variables, which is treated as an additional bounded disturbance to the energy space model. In Eqn. (5), the matrices and vectors utilized are:  $B_t = [0,4]^T$ ,  $B_z = [1 -1]^T$  for any component and matrix  $A_{z,i} = \begin{bmatrix} 0 & -1/\tau_i \\ 0 & 0 \end{bmatrix}$  depends only on the time constant  $\tau_i$  defined in Definition 6. Each of the control and disturbance ports are associated with respective interactions, denoted using superscripts u and m respectively as follows:  $\dot{z}_i^u = \begin{bmatrix} P_i^u, \dot{Q}_i^u \end{bmatrix}^T$  and  $\dot{z}_i^m = \begin{bmatrix} P_i^m, \dot{Q}_i^m \end{bmatrix}^T$  respectively. These vector entities comprise instantaneous power and rate of change of generalized reactive power that can be defined using respective ports' effort and flow variables as in Definitions 2 and 3 respectively [19, 32].

Next, the common output variable, i.e the interaction variable is defined in Eqn. (4b). It can only be numerically computed given the information of internal states

and its derivatives as shown in Eqn. (5b) [23]. This is represented through an abstract map  $\phi_{z,i}$ . Since outgoing interaction variable by Definition 1 is also a function of state derivatives (function of port input  $r_i$ ), the rate of change of outgoing interaction variable depends on the rate of change of incoming interaction variable. Such dependence makes the modeling framework inherently interactive. For more details on the interactive modeling approach, the reader is referred to [19, 18, 23].

**Remark 1.** The term  $\int_0^t E_{t,i}(s)ds$  in the energy space can be interpreted as the component of rate of change of energy that does useful work. In contrast the term  $\left(Q_i^{r,out} + Q_i^u + Q_i^m\right)$  corresponds to the component that contributes to inefficiencies (non-damping losses) associated with energy transfer. The former is called rate of change of exergy while the latter is called rate of change of anergy [2, 20]. For the purposes of TeDP control design, we claim that control designed to minimizing these dynamic inefficiencies results in better transient performance for challenging missions and could thereby substantially reduce the size of the engines.

Notably, the aggregate energy space model is linear in energy space variables. However, the model is dependent on internal variables in conventional space. The resulting interactive stand-alone component model, as shown in the schematic in Fig. 7 is not in a standard state space form. We emphasize that such modeling structure is inherent as claimed in Willems' seminal paper on behavioral modeling of physical systems [31].

#### 4.2. Stand-alone component model

We next introduce the zoomed-in component models. The physical models introduced in Eqn. (2) are related to the interaction variable and its dynamics, through a bi-directional dynamic mapping as shown in Fig. 7. From this figure, it is important to note that the physical lower layer model is characterized now using extended state space  $\tilde{x}_i = [x_i, m_i, r_i]^T \in \tilde{X}_i$ . Here, we characterize the persistent disturbances and incoming interactions at the ports through the instantaneous power and generalized reactive power at ports by the vector  $\dot{z}_i^m$  and  $\dot{z}_i^{r,in}$  respectively. An example of the zoomed-in representation of the multi-layered modeling for the candidate architecture in Fig. 1 is given in Section 4.3 We next discuss the specifics of the energy-based dynamical model.

In addition to the state dynamics, it now becomes imperative to model the dynamics of the disturbance and port inputs in order to include the dependence of instantaneous and reactive power entering the respective terminals  $(z_i^m, z_i^{r,in})$ . Characterization of these power variables, in turn, helps retain the linear structure of the

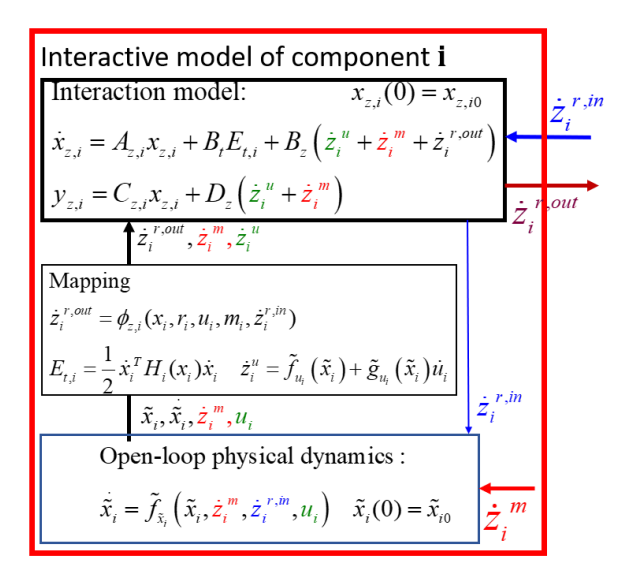


Figure 7: Interactive stand-alone model of an open-loop component i: The lower layer models are utilized to compute the outgoing interaction variable  $\dot{z}_{i}^{r,\text{out}}$ , which drive the higher-layer energy dynamics of the component. The incoming interaction variable from the grid  $\dot{z}_{i}^{r,\text{in}}$ , is utilized by the lower-layer models to evaluate the extended state trajectories  $\tilde{x}_i = [x_i, m, r_i]$  given their initial conditions.

higher layer energy space model in Fig. 7, also elucidated in Eqn. (5). The dynamics of extended state variables are expressed in Eqn. (6).

Extended state space model: 
$$\tilde{x}_{i}(0) = \begin{bmatrix} x_{i0} & m_{i0} & r_{i0} \end{bmatrix}^{T}$$

$$\begin{bmatrix} \dot{x}_{i} \\ \dot{m}_{i} \\ \dot{r}_{i} \end{bmatrix} = \begin{bmatrix} f_{x,i}(x_{i}) + g_{i}^{m}(x_{i})m_{i} + g_{i}^{r}(x_{i})r_{i} \\ f_{m,i}(\tilde{x}_{i}) + g_{m,i}^{m}(\tilde{x}_{i})m_{i} + g_{m,i}^{r}(\tilde{x}_{i})r_{i} \\ f_{r,i}(\tilde{x}_{i}) + g_{m,i}^{m}(\tilde{x}_{i})m_{i} + g_{r,i}^{r}(\tilde{x}_{i})r_{i} \end{bmatrix} + \begin{bmatrix} g_{i}^{u}(x_{i}) \\ g_{m,i}^{z}(\tilde{x}_{i}) & 0 \\ 0 & g_{r,i}^{zr}(\tilde{x}_{i}) & 0 \end{bmatrix} \begin{bmatrix} \dot{z}_{i}^{m} \\ \dot{z}_{i}^{z} \end{bmatrix} + \begin{bmatrix} g_{i}^{u}(x_{i}) \\ g_{m,i}^{u}(\tilde{x}_{i}) \\ g_{r,i}^{u}(\tilde{x}_{i}) \end{bmatrix} u_{i}$$

$$\tilde{f}_{\tilde{x}_{i}}(\tilde{x}_{i}, \dot{z}_{i}^{m}, \dot{z}_{i}^{z,in}, u_{i})$$
(6)

Here  $f_{x,i}, g_i^r, g_i^m$  are the same functions defined in Eqn. (2). The rest of the functions are a result of expressions for reactive power at respective ports according to Definition. 3.

## 4.3. Example of multi-layered modeling for DC system architecture

Consider the TeDP system in Fig. 1. The unified nature of the energy-based modeling lets each of the components be represented the same way as in Fig. 6. The lower layer physical dynamics block in extended state space and that of the mapping blocks in the zoomed-in representation however depends very much on the specific details of the components being modeled.

The physical dynamics of the component models in extended state space for DC generator (i = 1) and DC motor (i = 2) is shown in Eqn. (7).

DC machine stand - alone model:

$$\frac{di_{ai}}{dt} = -\frac{R_{ai}}{L_{ai}}i_{a1} + \frac{1}{L_{ai}}(v_{a1} - Ki_{fi}\omega_i) \ i_{ai}(0) = i_{ai,0} \ \ (7a)$$

$$\frac{d\omega_i}{dt} = -\frac{D_i}{J_i}\omega_1 + \frac{1}{J_i}\left(T_{mi} + K_i i_{fi} i_{ai}\right) v_{ai}(0) = v_{ai,0} \quad (7b)$$

$$\frac{di_{fi}}{dt} = -\frac{R_{fi}}{L_{fi}}i_{f1} + \frac{v_{fi}}{L_{fi}} \qquad v_{fi}(0) = v_{fi,0}$$
 (7c)

$$\frac{dT_{mi}}{dt} = \frac{d\omega_i}{dt} \frac{T_{mi}}{\omega_i} - \frac{1}{\omega_i} \dot{Q}_{mi} \qquad T_{mi}(0) = T_{mi,0} \qquad (7d)$$

$$\frac{dv_{ai}}{dt} = \frac{1}{2i_{ai}} \left( \hat{P}_i^{r,in} - \dot{Q}_i^{r,in} \right) \qquad v_{ai}(0) = v_{ai,0} \qquad (7e)$$

$$\frac{dv_{ai}}{dt} = \frac{1}{2i_{ai}} \left( \hat{P}_{i}^{r,in} - \dot{Q}_{i}^{r,in} \right) \qquad v_{ai}(0) = v_{ai,0}$$
 (7e)

Here, the Eqns. (7a) - (7c) represent the physical dynamics of generator or motor. The sign convention assumed is that the armature current is directed into the component. The right hand side of this model is represented as  $\tilde{f}_{\tilde{x}_i}$  in the general model in Eqn. (6). The disturbance  $T_{m2}$  in Fig. 1 needs to be modeled as a state to accommodate its time-varying properties depending on the information given. For the general disturbance characterization in Eqn.(1), the reactive power injected can be characterized as

$$\dot{Q}_{m2} = T_{m2}\dot{\omega}_2 - \omega_2 \dot{T}_{m2} 
= T_{m2,0} \left(\frac{\omega_2}{\omega_{2,0}}\right)^{\epsilon} \dot{\omega}_2 - T_{m2,0} \frac{\epsilon}{\omega_{2,0}} \left(\frac{\omega_2}{\omega_{2,0}}\right)^{\epsilon-1} \dot{\omega}_2$$
(8)

Depending on the type of disturbance characterization, we thereby have different dynamical evolution trajectories of the torque seen by the motor. On the other hand for the generator, the Eqn. (7) can be avoided for the open-loop model. An anologous dynamic map will be defined later in Section 6.

The Eqn. (7e) lets us characterize the interactions with the rest of the system. The incoming interaction variables are defined as the negative of the outgoing interaction variables of the neighbors as shown in Eqn. (9).

Zoomed – out interconnection relations : 
$$\dot{z}_1^{r,in} = -\dot{z}_2^{r,out} \qquad \dot{z}_2^{r,in} = -\dot{z}_1^{r,out} \qquad (9)$$

The outgoing interaction variables to be communicated to the neighbors for use in Eqn. (9) are computed by utilizing the map in Eqn. (5b) which is a result of definition of interaction variables in Eqn. (4b). The map  $\phi_{z,i}(\tilde{x}_i,\dot{\tilde{x}}_i,\dot{z}_i^{r,in})$  for the DC machine is given as follows:

Interaction variable computation:

$$P_{i}^{r,out} = \underbrace{L_{ai}i_{ai}\frac{di_{ai}}{dt} + L_{fi}i_{fi}\frac{di_{fi}}{dt} + J_{i}\omega_{i}\frac{d\omega_{i}}{dt}}_{P_{i}}$$

$$+ \underbrace{R_{ai}i_{ai}^{2} + R_{fi}i_{fi}^{2} + D_{i}\omega_{i}^{2} - \left(T_{mi}\omega_{i} + v_{fi}i_{fi}\right)}_{P_{i}^{u} + P_{i}^{m}}$$

$$\dot{Q}_{i}^{r,out} = 2\left(L_{ai}\left(\frac{di_{ai}}{dt}\right)^{2} + L_{fi}\left(\frac{di_{fi}}{dt}\right)^{2} + J_{i}\left(\frac{d\omega_{i}}{dt}\right)^{2}\right)$$

$$-\frac{d\hat{p}_{i}}{dt} - \left(T_{mi}\frac{d\omega_{i}}{dt} - \frac{dT_{mi}}{dt}\omega_{i} + v_{fi}\frac{di_{fi}}{dt} - i_{fi}\frac{dv_{fi}}{dt}\right)$$

$$\underbrace{Q_{i}^{u} + \hat{Q}_{i}^{m}}_{Q_{i}^{u} + \hat{Q}_{i}^{m}}$$

$$(10)$$

These maps are valid for both DC generator and motor. The internal extended state variables and their derivative are utilized to obtain the numerical values of  $\dot{z}_i^{r,out}$ . Note however that the expression above includes the computation of second derivative of stored energy as  $\frac{dp_i}{dt}$ . This requires computation of second derivative of state variables, which may not be readily available and thus are estimated using previous available values. Furthermore, the vector  $\dot{z}_i^{r,in}$  has the components of instantaneous power and generalized reactive power rate, the rate of change of instantaneous power for use in Eqn. (7e) is also estimated through the usage of previous timestep values and is thus denoted with a hat symbol.

Notice that the modeling method is inherently interactive in nature, which is required for distributed control design. It has a linear structure as viewed by the higher layer unified energy space model in Eqn. (5a) for i = 1, 2 and Eqn. (9). However, the stand-alone component models interacting with higher layer models require advanced numerical methods, which is outside the scope of this paper. The reader is referred to [13] for additional details on some preliminary numerical methods.

# 5. Distributed feasibility and stability conditions in energy state space

The modeling approached introduced in the previous section accounts for the interactions with the rest of the system. It lends itself to distributed control design and also facilitates control co-design approach. The discussion of latter will be postponed to next section. In this section, we assume given the incoming interaction variables into the component, and design a distributed stabilizing controller possibly with additional objectives of

regulation of output variables of interest. Sufficient conditions on feasibility and stability of the resulting closed loop model will further be derived.

#### 5.1. Stand-alone component control:

The proposed control design approach involves two steps:

- Higher-layer reactive power control: In this layer, we utilize the linear energy space model shown in Eqn. (5a) to design the generalized reactive power injected into the control terminals with an objective of aligning the outgoing interaction variables with the incoming reactive power.
- Lower-layer implementation: The task of implementing the higher layer reactive power flow is carried over in this layer. Additional objectives of the regulation of output variable dictating quality of service can further be accommodated in this layer as needed.

The block diagram of the proposed design scheme is shown in Fig.

The higher layer design is performed by selecting an output variable  $y_{z,i}$  in energy space as follows:

$$y_{z,i} = \frac{E_i}{\tau_i} - P_i^u - P_i^m \tag{11}$$

This variable corresponds to the energy absorbed or injected by the component after energy dynamics settle, i.e.  $p_i = 0$ . By taking its time derivative and plugging in the relations given by the interaction model in Eqn. (5a), we have the dynamic input-output relation between the second component of input  $\dot{z}_i^u$  and the chosen output  $y_{z,i}$  as shown in Eqn. (13).

$$\dot{y}_{z,i} = \frac{p_i}{\tau_i} - \dot{P}_i^m - \dot{P}_i^u = -\dot{p}_i + \dot{P}_i^{r,out}$$

$$= \underbrace{\left(-4E_{t,i} + \dot{P}_i^{r,out} + \dot{Q}_i^{r,out} + \dot{Q}_i^m\right)}_{p_i(\bar{x}_i, \dot{\bar{x}}_i; \dot{z}_i^m)} + \underbrace{\dot{Q}_i^u}_{u_{z,i}}$$
(12a)

Based on this model, we proposed a feedback linearizing control in energy space with a positive gain  $K_i > 0$  as in Eqn. (12b).

$$u_{z,i} = -\eta_i(\tilde{x}_i, \dot{\tilde{x}}_i, \dot{z}_i^m) - K_i(y_{z,i} - y_{z,i}^{ref}) + \dot{y}_{z,i}^{ref}$$
 (12b)

We select  $y_{z,i}^{ref} = P_i^{r,in}$  so that the component aligns with the rest of the system upon interconnection. In practice, the variable  $\eta_i$  need not be known exactly. Even if the bounds on the nonlinearity in the energy space

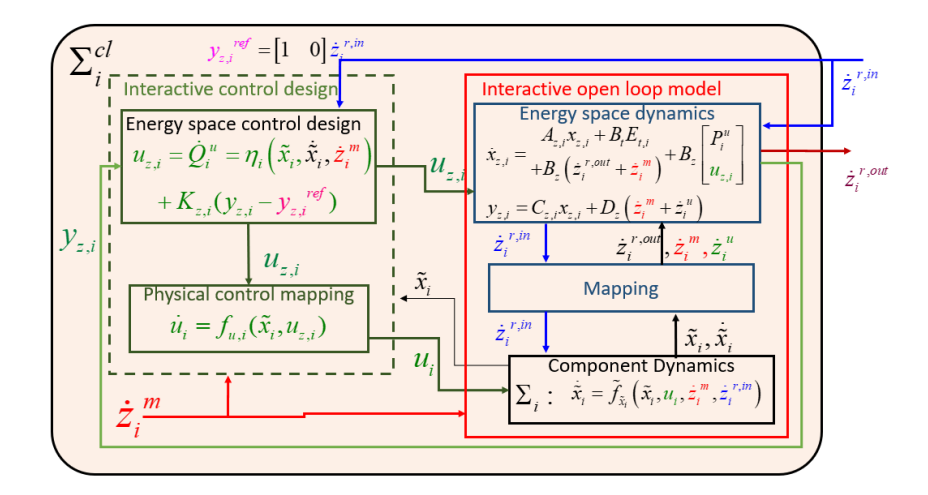


Figure 8: Block diagram of closed loop module formed by component-level distributed interactive control. The measurements of the energy produced by the component after energy dynamics settle  $y_{z,i}$  is utilized in the higher layer to dictate the generalized reactive power that is needed to regulate its value to a consistent reference values  $y_{z,i}^{ref} = P_i^{r,in}$ . This reactive power is implemented in the inner loop (lower layer) by utilizing internal extended state space variables  $\tilde{x}_i$ 

are known, an alternative sliding mode implementation can be performed, which altogether obviates the need to measure internal state variables and the derivatives. For details, the reader is referred to [22].

The corresponding higher layer design  $u_{z,i}$  can then be mapped to the physical control by utilizing the definition of reactive power in Definition 3 and then rearranging the terms, resulting in Eqn. (14).

$$\dot{u}_{i} = \frac{\dot{w}_{i}^{u}}{w_{:}^{u}} u_{i} - \frac{1}{w_{:}^{u}} u_{z,i} = f_{i}^{u}(\tilde{x}_{i}, u_{z,i})$$
 (12c)

Here  $w_i^u$  is the dual variable associated with the control input. For example, if torque is the control input, its dual variable will be the state at the same port, which is the angular velocity. Note that the map  $f_i^u$  is well defined since  $w_i^u$  is non-zero for non-zero higher layer design variables  $\dot{z}_i^u = [P_i^u, \dot{Q}_i^u]$ .

Notably, irrespective of the internal details of the components in any TeDP architecture, the higher layer design can be performed in a unified way. Only minimal information on the port variables of control terminal are needed for physical control implementation. The control design introduced in this section not only leads to provable stability upon interconnection, but also lead to efficient utilization of controllers. This is because the interactive control at any time instant cancels the residual reactive power at interfaces thereby minimizing the dynamical inefficiencies. Furthermore, the reference values utilized by the higher layer facilitate coordinated control between the components. This is in sharp

contrast to the stand-alone component control design that is performed under the assumption of weak coupling, or competitive disturbance rejection or feedbacklinearization based schemes.

## 5.2. Sufficient component-level conditions

The proposed two-layered design can also be interpreted as an input-output linearization based control. The input-output linearized model in closed loop can be written as in Eqn. (13).

$$\dot{y}_{z,i} = -K_i \left( y_{z,i} - y_{z,i}^{ref} \right) + \dot{y}_{z,i}^{ref}$$

$$\dot{\tilde{x}}_i = \tilde{f}_{\tilde{x}_i}(\tilde{x}_i) + \tilde{g}_{\tilde{x}_i}^m(\tilde{x}_i) \dot{z}_i^m + \tilde{g}_{\tilde{x}_i}^r(\tilde{x}_i) \dot{z}_i^{r,in}$$

$$+ \tilde{g}_{\tilde{x}_i}^u(\tilde{x}_i) U_i(\tilde{x}_i, P_i^m, y_{z,i})$$
(13b)

Here, the map  $U_i(x_i, P_i^m, y_{z,i}) \to u_i$  is defined as in Eqn. (14) to obtain physical control  $u_i$  given the output variable in energy space.

$$u_{i} = \frac{1}{w_{i}^{u}} \left( \frac{E_{i}(x_{i})}{\tau_{i}} - y_{z,i} - P_{i}^{m} \right)$$
 (14)

The input-output model in Eqn. (13) has a relative degree equal to one since the first time derivative of the output is directly dependent on the control in energy space  $u_{z,i} = Q_i^u$ . The rest of the state variables characterizing the internal dynamics, are not directly affected by the virtual control in energy space  $u_{z,i}$ . They are only affected by physical control  $u_i$ , which is re-expressed through the map  $U_i(x_i, P_i^m, y_{z,i})$ .

It is often useful to analyse the normal form form to understand the input-output behavior of closed-loop component models. Normal form models follow the same properties as the original model in closed loop only if there exists a diffeomorphism between the two [9]. Since the relative degree of the input-output linearized model is 1, the existence of the bijective map between  $u_i$  and  $y_{z,i}$  given by Eqn. (14) and (11) is sufficient to prove the diffeomorphism [22]. We thus utilize the normal form model for the stability analysis in our claim for sufficient stability conditions.

## **Theorem 1.** (Stability of closed-loop model)

Consider the virtual control  $u_{z,i}$  designed as in Eqn. (12b). and the closed loop model formed by equations (6), (12c) with the output variable definition in Eqn. (11) and the reference value  $y_{z,i}^{ref} = [1,0]\dot{z}_i^{r,in} = P_i^{r,in}$ . Assume existence of unique equilibrium  $\tilde{x}_i^*$  for each value of  $\dot{z}_i^{r,in}(t) \forall t$ , the quasi-static equilibrium thus obtained is stable in the sense of Lyapunov if the rate at which useful energy gets generated by the component is less than the tracking error.

$$\int_{0}^{t} 4E_{t,i}(s)ds \le \left(y_{z,i}(t) - y_{z,i}^{ref}(t)\right) \tag{15}$$

*Proof.* The proof is detailed in Appendix D. 
$$\Box$$

When two or more components are left to interact, the incoming interaction variable drives the system dynamics. It changes the natural equilibrium of the standalone component model to that of the interconnected system model. However, this dynamic adjustment at the interfaces is contingent upon the existence of interconnected system equilibrium and the dynamical exchange of power across components. As a result, there are two related questions that are to be answered: (i) if there exists an interconnected system equilibrium and (ii) if the such equilibrium is stabilizable. The theorem 1 answers the second question in part assuming there exists an equilibrium for each incoming interaction variable from the rest of the system. We next address the first question assuming the sufficient stability conditions are satisfied, i.e. we derive conditions under which the component can be connected to the rest of the system. We finally propose a control co-design method that accounts for the interdependencies in Section 6,

## 5.3. Sufficient system-level conditions

The interaction variables shared between components may interactively settle down to a common value resulting in a system equilibrium or may become unstable. We propose sufficient feasibility conditions that can be checked by each component in a feed-forward way to ensure feasible interconnection. In closed loop, the energy space model representation observes dynamical model as in Eqn. (16).

Interaction model in closed loop: (16) 
$$\dot{x}_{z,i} = A_{z,i}x_{x,i} + B_tE_{t,i} + B_z\dot{z}_i^{r,out} \quad x_{z,i}(0) = x_{z,i0}$$

The matrices  $A_{z,i}$ ,  $B_t$ ,  $B_z$  are the same as defined for Eqn. (5). It should be noted that  $\dot{z}_i^{r,out}$  and  $E_{t,i}$  here are functions of local energy conversion dynamics, the trajectories of which evolve as per the extended space model in closed loop dictated by Eqn. (6), (12b) and (12c).

Let us first characterize the variation of incoming and outgoing interaction variables over a period of time  $t \in [kT, (k+1)T]$  in the sets  $\mathcal{Z}_i^{r,in}[k]$  and  $\mathcal{Z}_i^{r,out}[k]$  respectively. Here,  $T >> t_r$  where  $t_r$  is the settling time of input-output model in Eqn. (13a). The settling time of the output variable in energy space is approximately five times the time constant of the closed loop input-output model, which is equal to  $\frac{5}{K_i}$ . Alternatively, an equivalent sliding mode control was proposed in [22] which has finite settling time properties.

We propose that each component based on previous time period  $Z_i^{r,in}[k-1]$ , compute the set  $Z_i^{r,out}[k]$  by utilizing the relation in Eqn. (13a). Thus characterized sets are then communicated to neighbors and then at the present time period, the set of incoming interaction variable at each of the components is computed as

$$\mathcal{Z}_{i}^{r,in}[k] = \left\{ -\sum_{j \in C_{i}} z_{j}^{r,out} \middle| z_{j}^{r,out} \in \mathcal{Z}_{j}^{r,out}[k] \right\}$$

Numerical algorithms to characterize the sets of outgoing interaction variables are a topic of future research. In this paper, we assume these sets can be computed ahead of time by each component.

We propose a sufficient condition utilizing these sets computed in a look-ahead manner for each time interval T to claim general dissipativity result that holds for time  $t \in [kT, (k+1)T]$ .

**Lemma 1.** (Feasibility of component interconnection) If the set  $Z_i^{r,out}[k]$  as characterized by the closed loop interactive model of  $\Sigma_i$   $\forall z_i^{r,in}(t) \in Z_i^{r,in}[k]$  observes the condition  $Z_i^{r,out}[k] \subseteq Z_i^{r,in}[k]$ , then,  $\Sigma_i$  is dissipative with respect to the supply function  $(\dot{P}_i^{r,in}(t) + \dot{Q}_i^{r,in}(t)) \forall t \in [kT, (k+1)T]$ .

*Proof.* The proof is elaborated in Appendix E.  $\Box$ 

Each of the components satisfying Lemma 1 implies that there exists an interconnected system equilibrium  $x_i^*(t) \forall i$  as viewed by each of the components. Such equilibrium is possibly time-varying but is stabilizable under the conditions stated in Theorem 1. Furthermore, the general dissipativity result in Lemma Appendix E is additive across components which leads to the following interconnected system stability result.

**Theorem 2.** (Stability of interconnected system) Assume  $\Sigma_i$  in closed loop at each time t observes the properties stated in Theorem  $1 \forall z_i^{r,in}(t) \in \mathcal{Z}_i^{r,in}[k]$ . Assume further that the pre-chraracterized sets of interaction variables satisfy sufficient feasibility conditions stated in Lemma 1. Several such components interacting with each other through memory-less junctions result in an interconnected system that is stable in the sense of Lyapunov  $\forall t \in [kT, (k+1)T]$ .

*Proof.* The proof is provided in Appendix F,  $\Box$ 

After the energy dynamic transients settle i.e. when  $\dot{E}_i = p_i = 0$ , the feasibility conditions imply that the error  $\left(y_{z,i} - y_{z,i}^{ref}\right) < 0$ . This condition is also consistent with the sufficient feasibility condition, since the stored energy in tangent space is always positive. The two conditions therefore result in perfect alignment of interaction variables viewed from the perspective of both component-level and system-level. The feasibility conditions are intended to be checked in a feed-forward way which is elaborated upon next. They can also be accommodated in a look-ahead centralized controller with dynamical energy space constraints [14] for optimal trajectory planning. However, such an extension is out of the scope of this paper.

# 6. Towards control co-design for provable performance of TeDP systems

The new energy space modeling and control approach lends itself well to integrating control design at early stages of system design [11]. Proposed control codesign is qualitatively different from today's testing whether each stand alone component meets specifications measured in terms of frequency and voltage response for given ranges of loads [26]; recall from Appendix A that these tests are insufficient to ensure expected system-wide interaction dynamics. Instead, the control design is iterative process in which there exists a trade-off between making module-level control follow specifications and system-level design realizing that the components can not meet specifications and the need for new equipment. For example, torque control may

not be sufficient. So TeDP designer may add storage to follow the mission. More traditional approach is to add large capacitance as a buffer between components to ensure components meet certain specifications. Instead approach here is an interactive control co-design in which different alternatives between more enhanced component control and the need for adding more storage or large capacitors. It comprises following steps [11]:

- Step 1: Design control of each module to meet best possible performance characterized and measured in terms of its interaction variables
- Step 2: Assess whether the interactions between the modules with given specifications result in system-wide dynamics that is feasible within the engineering specifications, stable and robust
- Step 3: Simulate and analyze whether the system performance on scenarios given by the user for the worst case scenario is as expected.
- Step 4: If not, iterate starting from Step 1.
- Step 5: Stop when performance is acceptable.

In this paper we pursue this control co-design approach by starting with the candidate TeDP architecture of interest and given its performance (providing timevarying torque to propulsors, for example). Given candidate hardware components (generators, motors) and candidate architecture like the ones shown in Figures 2 and 3, the architecture is decomposed into sub-systems and the performance of each sub-system is modeled and assessed in terms of its ranges of interaction Variables. Different control methods are assessed for their impact on the ranges of power, rates of change reactive power and energy over the given time horizon, as illustrated in Section 7.1 next. Next, feasibility and stability are assessed in a feed-forward way for the next time horizons using conditions described in Section 5. If these conditions are not met, enhancements of subsystem controllers can be pursued and/or new components, such as larger capacitors, power electronicallycontrolled switches for controlling reactive power dynamics in addition to mechanical torque control, or eventually even real battery storage may be added. Since system-level assessment is done in linear energy state space, it becomes possible to have provable feasibility and stability conditions. In short, pursuing Step 1 in conventional state space, and Step 2 using higher level energy state space modeling supports iterative control co-design approach for provable performance eve in these otherwise complex nonlinear MIMO TeDP dynamical systems. Moreover, since testing for feasibility and stability can be done using only local state variables and interaction variables, cooperative distributed semi-autonomous performance is supported by the subsystems comprising these systems. The controllers are robust with respect to communications failures, and this further ensures more safe performance which is one of the most critical aspects of control design for aircrafts.

#### 7. Illustrative TeDP systems

Any machine model constituting the TeDP system has a general electromechanical structure as explained in Appendix B which can be utilized to pose the control problem in a unified manner as explained in Section 5. In this section, we specifically consider the TeDP architecture in Fig. 2 for illustrations. The parameters of the system considered are provided in Appendix G.

In section 7.1, we first assess if the traditional control co-design approach explained in Section 6 can still ensure interconnected system stability. We provide an elaborate comparative simulation results of state of the art approaches and that of energy-based control. Next in section 7.2, we consider a more challenging timevarying torque disturbances corresponding to different requirements of the fan connected to the motor shaft as in Eqn. (1). We show proof-of-concept effectiveness of our proposed energy-based control co-design relative to state of the art approaches for the the simplest TeDP architecture in Fig. 1.

## 7.1. Control co-design for static changes

The traditional control co-design involves each standalone machine control tuned for each step change in the expected disturbance in the best possible way. Often the anticipated disturbances from rest of the system are modeled as a Thevinin's equivalent impedance for which the tuning of controller is done. The resulting interconnected TeDP system is then anticipated to remain stable.

We first consider the step change in power disturbances ( $\epsilon = -1$  in Eqn. (1)) as shown in Fig. 9. This torque seen by  $\Sigma_2$  in any of the TeDP architectures approximately manifest as the power disturbances seen by  $\Sigma_1$  at the interface for negligible damping losses in  $\Sigma_2$ . The stand-alone tuning of  $\Sigma_1$  in traditional control codesign approach is done for an equivalent Thevenin's resistance constructed at the terminals assuming nominal voltage of 1p.u..

Assuming negligible damping losses, the permanent magnet generator is tuned best possible way for each of

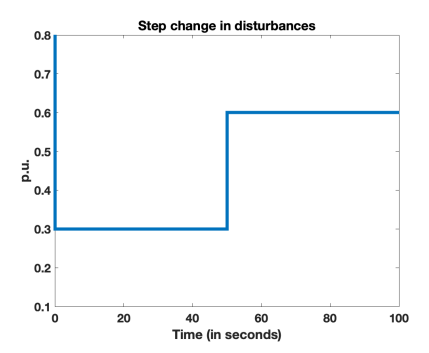


Figure 9: Step change in disturbances entering the TeDP system: These are mechanical power values required by the fan connected to the motor shaft.

the step changes in power. We consider two different control approaches. The first is the common governor control of generator responding to the error in output of importance. Traditionally the chosen output is frequency which leads to the PID control as in Eqn. (17) with  $y_1 = \omega_1$ . The second is the full state feedback control as in Eqn. (18).

$$u_{1} = -K_{p1} \left( y_{1} - y_{1}^{ref} \right) - K_{i1} \int_{0}^{t} \left( y_{1} - y_{1}^{ref} \right) dt - K_{di} \frac{dy_{i}}{dt}$$

$$u_{1} = -K_{1} \left( x_{1} - x_{1}^{*} \right) + u_{1}^{*}$$
(18)

Here once again  $u_1$  is the torque applied and the states to which control responds is the entire state vector of permanent magnet generator i.e.  $x_1 = \begin{bmatrix} \delta_1, \omega_1, i_{Sd1}, i_{Sq1} \end{bmatrix}^T$ .  $x_1^*$  and  $u_1^*$  respectively are the equilibrium and the input corresponding to equilibrium for each of the step changes considered. Since the entire state vector equilibrium for each step change can not be know exactly, we utilize the equilibrium corresponding to the first step.

Most importantly, the state of the art controller design methods can not be utilized to directly regulate voltage. However, with energy-based control, the output variable and its reference value in energy space has been changed to accommodate regulation objectives as follows:

$$y_{z1} = \underbrace{R_1 \begin{pmatrix} i_{d1}^2 \\ +i_{q1}^2 \end{pmatrix} + (F_1 + K_{\omega}) (\omega_1 - \omega_0) \omega_1}_{E_1/\tau_1} - \underbrace{T_{m1}\omega_1}_{P_1^u}$$

$$y_{z1}^{ref} = P_1^{r,in} K_{\nu} \frac{V^{ref}}{V}$$

$$= \left(v_{d1}i_{d1} + v_{q1}i_{q1}\right) K_{\nu} \frac{V^{ref}}{\sqrt{v_{d1}^2 + v_{q1}^2}}$$
(19)

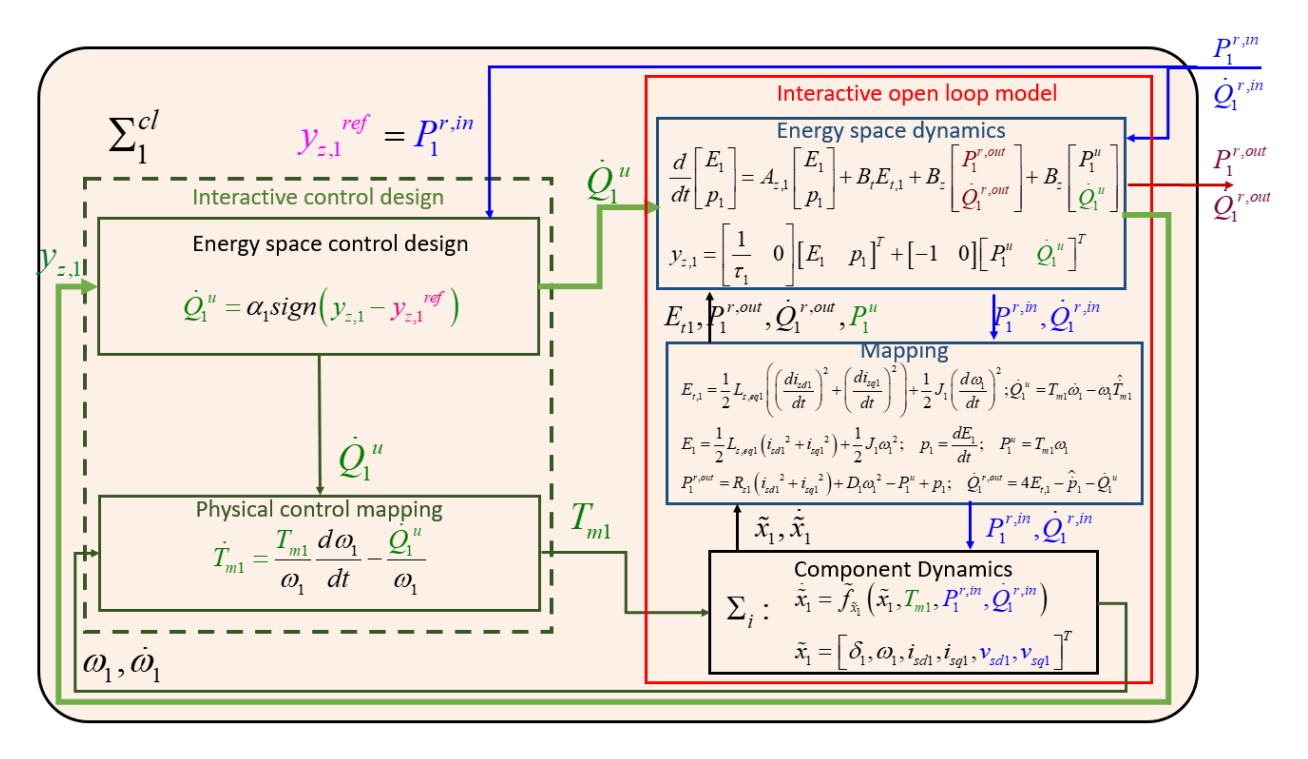


Figure 10: Block diagram of closed loop permanent magnet generator module with component-level distributed interactive control. The measurements of the energy produced by the component after energy dynamics settle  $y_{z,1}$  is utilized in the higher layer to dictate the generalized reactive power that is needed to regulate its value to a consistent reference values  $y_{z,1}^{ref} = P_1^{rin}$ . This reactive power is implemented through the torque control in the lower layer by utilizing the information of angular frequency and its derivative

Here the gains  $K_{\omega}$ ,  $K_{\nu} > 0$  dictate the tradeoff between the frequency regulation and voltage regulation objectives respectively. These output variables in energy space are utilized for torque control through a dynamic control mapped as in Eqn. (12c) which for the example of permanent magnet generator leads to:

$$\frac{dT_{m1}}{dt} = \frac{T_{m1}}{\omega_1} \frac{d\omega_1}{dt} - \frac{1}{\omega_1} u_{z1}$$
where
$$u_{z1} = \alpha_1 \operatorname{sign} \left( y_{z1} - y_{z1}^{ref} \right)$$
(20)

Here the energy space design is implemented through a sliding mode equivalent control, in contrast to the general feedback linearizing control stated in Eqn. (12b). The sliding mode gain  $\alpha_1$  is the upper bound on the nonlinearities  $\eta_1$  defined in Eqn. (13a). Interested readers are referred to [22] for more details on the equivalent sliding mode control.

The general control block diagram shown in Fig. 8 for the particular case of permanent magnet generator without considering regulation objectives is summarized in Fig. 10. Notice that some of the energy space variables denoted with a '' need to be estimated using previous available measurements as explained for the

DC machine example in Section 4.3. This is because of the inherently interactive dynamic model of the component. The lower layer physical model of permanent magnet generator is given in Eqn. (B.4) which is utilized to compute energy variables needed for the higher layer model and control design. The extended state dynamics corresponding to the voltage variables is given by the following set of dynamical equations:

$$\frac{d}{dt} \left[ \underbrace{v_{d1}}_{v_{q1}} \right] = \left[ \begin{array}{c} \omega_0 v_{q1} \\ -\omega_0 v_{d1} + \frac{\hat{P}_1^{r,in} - (Q_1^{r,in} - 2\omega_0(v_{q1}i_{d1} - v_{d1}i_{q1}))}{2P_1^{r,in}/(\sqrt{v_{d1}^2 + v_{q1}^2})} \end{array} \right]$$
(21)

These relations are a result of definition of instantaneous power and generalized reactive power in rotating reference frame. The derivation is out of scope of this paper. Notice that from an implementation standpoint, the only measurements needed are that of energy space variables  $y_{z,1}$  for higher layer design and the angular frequency and its derivative for the lower layer implementation.

The resulting stand-alone response of the generator

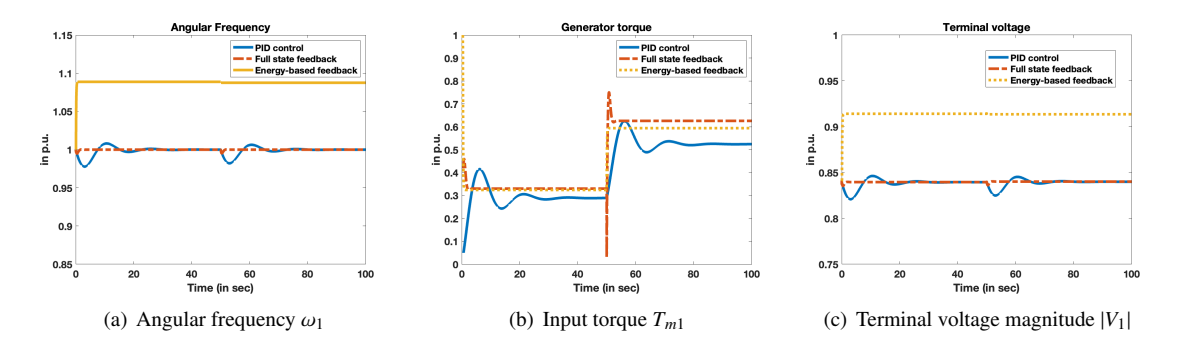


Figure 11: Comparison of generator trajectories for the armature power disturbances in Fig. 9 with PID control (Eqn. (17)) in blue; LQR control (Eqn. (18)) in red and energy-based control (Eqn. (20)) in yellow.

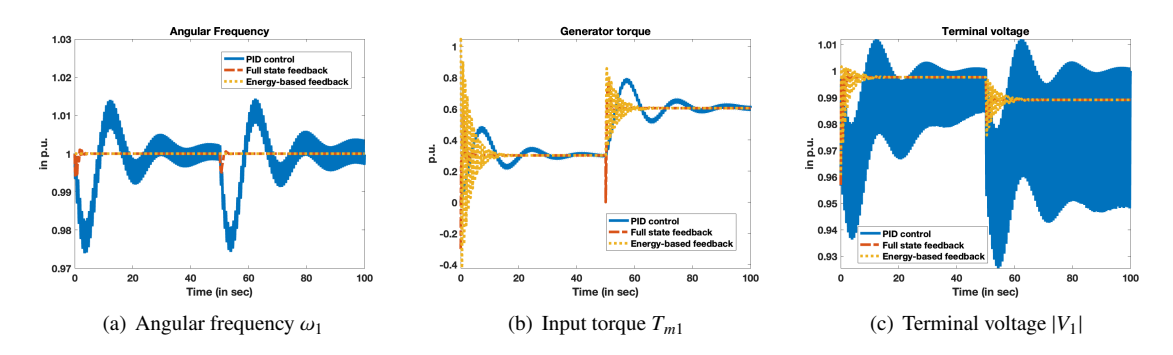


Figure 12: Comparison of generator trajectories when connected to the motor with propulsor disturbances in Fig. 9 with PID control (Eqn. (17)) in blue; LQR control (Eqn. (18)) in red and energy-based control (Eqn. (20)) in yellow.

frequency when compared to the state of the art methods is shown in Fig. 11(a). It can be seen that the transient overshoots are much lower with energy-based design. It is extremely hard to tune the PID control for a given step change in power disturbances. Hence in these plots, we have obtained the trajectories for a equivalent Thevenin's resistance at the armature representing the given armature disturbance. As a result, the control torque applied in steady state for the second step change is slightly different with the PID control as shown in Fig. 11(b). Much more important is to note that there is a slight frequency offset with energy-based control in Fig. 11(a), which is because of the voltage regulation objective considered in the design. For  $K_{\nu} = 60$  and  $K_{\omega} = 100$  in the design in Eqn. (19), the voltage trajectories are shown in Fig. 11(c).

Next, when the stand-alone permanent magnet generator is connected to the motor that is actually subject to the disturbances in Fig. 9, the interconnected system frequency trajectories are shown in Fig. 12(a). It is expected that the interconnected system response is similar to the stand-alone component response. But clearly there are some oscillatory modes that persist in the interconnection system with PID control resulting from

the interconnection. For certain operating conditions, these oscillations could be as large that they could even potentially destabilize the interconnected system.

Comparing the other two controllers in the interconnected system, it can be seen from Fig. 12(b) that the LQR control settles slightly faster than the energy-based control, but it however has significantly larger transient overshoots. The voltage trajectories of the interconnected system surprisingly result in voltages close to 1 p.u. as shown in Fig. 12(c) which was not achievable with stand-alone component tuning with conventional methods. From these plots, we can conclude that conventional control co-design methods may lead to erroneous conclusions on interconnected system response. It could also potentially lead to over designing of the engine in the TeDP system. In contrast the energy based controllers are designed with an objective of aligning power interactions with rest of system, thereby resulting in similar stand-alone and interconnected system re-

Next we consider a time-varying disturbance that could potentially enter the TeDP systems especially when subject to challenging aircraft missions.

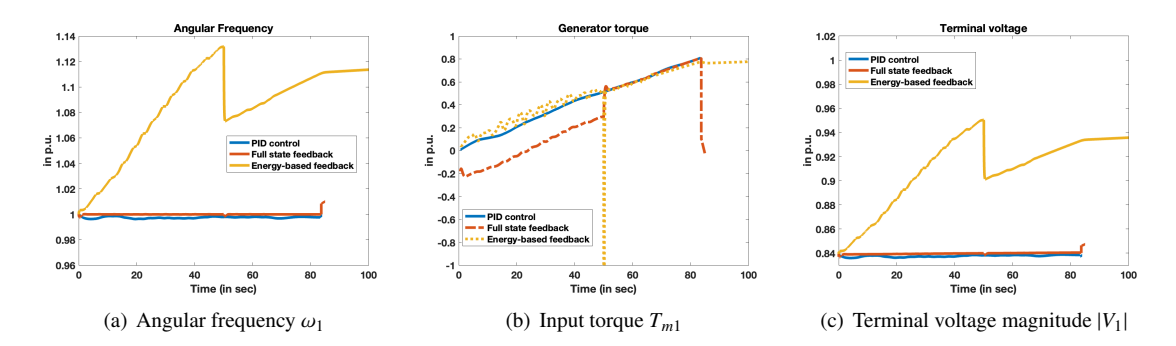


Figure 13: Comparison of generator trajectories for the armature power disturbances in Fig. 15 with PID control (Eqn. (17)) in blue; LQR control (Eqn. (18)) in red and energy-based control (Eqn. (20)) in yellow.

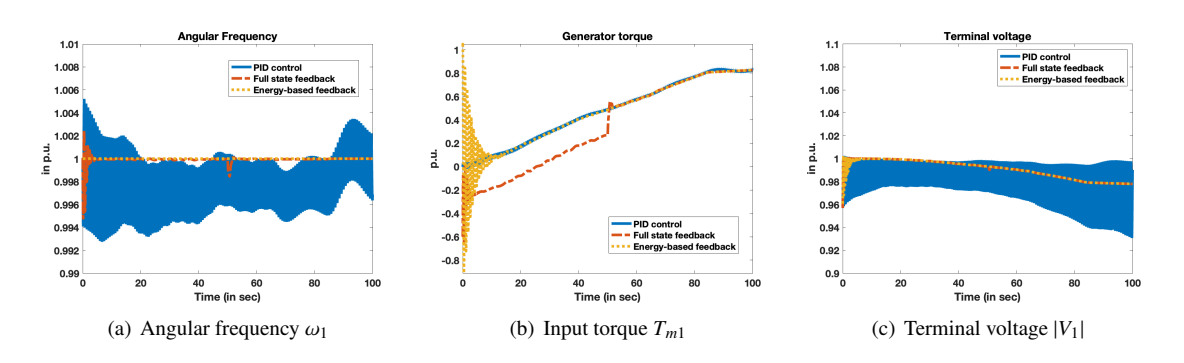


Figure 14: Comparison of generator trajectories when connected to the motor with propulsor disturbances in Fig. 15 with PID control (Eqn. (17)) in blue; LQR control (Eqn. (18)) in red and energy-based control (Eqn. (20)) in yellow.

## 7.2. Control co-design for continuous changes in load

For this case study we consider the time-varying power disturbances corresponding to  $\epsilon = -1$  in Eqn. (1) as shown in Fig. 15. In the previous sub-section,

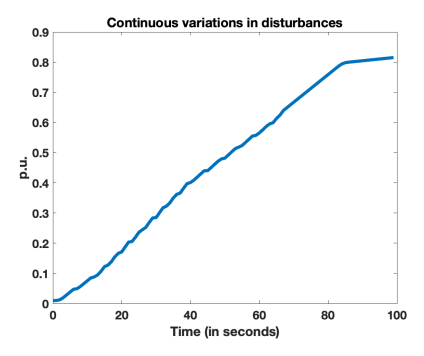


Figure 15: Disturbances entering the TeDP system: These are mechanical power values required by the fan connected to the motor shaft

the control co-design was performed for 50 second averaged values of power disturbances in Fig. 15. For the continuous variations however, since re-tuning of con-

trollers can not be formed at every instant, we utilized re-tuned gains only at t = 0 and t = 50. The resulting stand-alone mode responses are shown in Fig. 13.

The LQR and PID controllers fail at 85th second due to voltage instability created by constant power disturbances. In contrast, the interconnected system responses with conventional control methods are stable with a co-incidentally good frequency and voltage regulation as shown in 14.

From this exercise, we can conclude that we cannot achieve provable performance with the conventional controllers tuned in stand alone mode upon interconnection. This happens because the constant power disturbances seen by generator get filtered through the natural dynamics of the motor. Such effects are to be explicitly considered through the modeling of interaction dynamics. We do so with energy based controllers and thus the trajectories are stable at any operating point in both stand-alone and interconnection modes. The voltage and/or frequency regulation is treated as a secondary control objective over slower timescales and thus perfect regulation could not be achieved in stand alone mode. Furthermore, the incoming reactive power dy-

namics are assumed to correspond to the worst case value corresponding to a constant power sink with zero inertia. However, in the interconnection mode, the inertia of rest of the system in not zero in reality. Thus, the response only gets better as seen in Fig. 14, depending on the value of inertia of the rest of the system.

If the voltage or frequency regulation is an important specification that ought to be satisfied in stand-alone mode, one approach is to have an accurate representation of the incoming reactive power from the rest of the system. Alternatively, additional hardware that can provide extra degree of control can be added in. For example, if we consider the power electronics interface such as the one shown in Fig. 3, we can achieve potentially achieve better frequency and voltage regulation even in stand-alone modes. This is a topic of future research.

#### 8. Summary and future work

We have proposed a control co-design method that involves feed-forward conditions on energy variables for feasible interconnection. These conditions result from the distributed multi-layered interactive energy-based control that is technology-agnostic. The component-level design focuses on minimizing the dynamic inefficiencies associated with power transfer between the components thus leading to smarter utilization of available control hardware. The feed-forward sufficient conditions are distributed and easy-to-check by the components themselves.

Alternatively, a system-level controller can check for these conditions. Upon violation, minimal hardware to be procured can be identified. For example TeDP system considered in Section 7, if the disturbance magnitudes were ten times larger, the existing hardware is not sufficient since the feasibility conditions may get violated. When such infeasibilty is detected, it is the job of system-level controller to activate additional hardware. Corresponding system-level problem can be posed to even identify minimal storage needed to still accommodate ten times large disturbance. While this paper provides the tools to facilitate provable control co-design as explained in Section 6, problem posing for the tradeoff analysis between the hardware sizing and smart actuators for different mission requirements need to still be pursued.

Another promising direction of future research is to ensure sufficient stability condition in Eqn. (15). In the current control design method, it is assumed that such condition is satisfied, which is even hard to check ahead of time. We have proposed an alternative model in [14] where the exergy dictating variable  $E_{t,i}$  is treated

as a state variable in conjunction with the model in Eqn. (5a). The corresponding third-order energy space model for a single port component is given in Eqn. (22).

$$\frac{d}{dt} \underbrace{\begin{bmatrix} E_i \\ p_i \\ E_{t,i} \end{bmatrix}}_{x_{z,i}} = \begin{bmatrix} 0 & 1 & 0 \\ 0 & 0 & 4 \\ -\frac{1}{\tau_i} & 0 & 0 \end{bmatrix} x_{z,i} + \begin{bmatrix} 0 & 0 \\ -1 & 0 \\ 0 & 1 \end{bmatrix} \underbrace{\begin{bmatrix} \dot{Q}_i^u \\ P_{t,i}^u \end{bmatrix}}_{u_{z,i}} \tag{22}$$

This model also has additional degree of control in energy space called power in tangent space  $P_{t,i}^u$  which can be utilized to ensure satisfaction of sufficient stability condition. If instantaneous power at control port  $P_i^u$  is defined as  $v_i i_i$ , then  $P_{t,i}^u$  is defined as  $\frac{dv_i}{dt} \frac{di_i}{dt}$ . This model can especially be useful in power electronics based control where fast switching control is permissible.

## Acknowledgments

This paper is a result of collaborative work between New Electricity Transmission Software Solutions (NETSS) and NASA Glen Research Center. Technical input and guidance by Raymond Beach and his colleagues have been invaluable. Financial support under the SBIR Phase 2 NETSS Project on "Integrated Control and Protection Methodology Based on Energy-Space Modeling for EAP Aircraft" Contract number 80NSSC20C0092 and partial funding by the NSF EArly-Concept Grants for Exploratory Research (EA-GER) "Fundamentals of Modeling and Control for the Evolving Electric Power System Architectures" project ECCS-2002570 have made this effort possible, and it is greatly appreciated. The NETSS and MIT colleagues Eric Allen, James Kirtley and Jeffrey Lang provided much guidance regarding the state-of-the-art control of electrical machines.

## Appendix A. New challenge of tuning controllable equipment

Consider a simple R-L circuit element with a controllable voltage source that supplies a constant power as shown in Fig.A.16. The inductor and resistor in Fig.

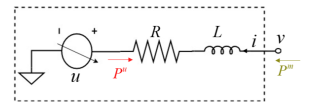


Figure A.16: Motivating example: Controllable lossy inductor

A.16 represent the inertia and damping of any component under consideration. The inductor is associated

with a state variable current i, and the voltage source injects a controllable power  $P^u = ui$  for the disturbances seen at its interface  $P^m = vi$ . The net power that can be injected by the controllable sources shown in green in Fig. 1 can be abstracted as controllable power  $P^u$  while the one that the fans powering the mission absorb can be abstracted as net uncontrollable power disturbances  $P^m$ . With this resemblance between the general TeDP system in Fig. 4 to that in Fig. A.16 established, we illustrate the inherent operating problems when subject to time-varying interactions by showing the simulation response of the circuit in Fig. A.16.

From an energy standpoint, the initial stored energy in the inductor of the representative circuit in Fig. A.16 is given by the initial current  $i_0$ , as  $E_0 = \frac{1}{2}Li_0^2$  is supposed to decay exponentially, the rate of which is dictated by the system damping if the controlled power  $P^u$  is designed to exactly counteract  $P^m$  at each time instant. Simple energy conservation principles give the governing dynamics as follows:

$$\dot{E}(t) = -Ri^2 + P^m(t) + P^u(t) \qquad E(0) = \frac{1}{2}Li_0^2 \quad (A.1a)$$
$$= -\frac{2R}{L}E + P^m(t) + P^u(t) \qquad (A.1b)$$

The common control methods such as pole placement technique that can be employed in Fig. A.16 can be interpreted using the following control strategy [7].

$$P^{u}(t) = -KE(t) + P^{m}(t - \delta t)$$

This control  $P^u(t)$  is implemented as a discrete time control. The second component is a feed-forward signal to balance the power at equilibrium. It is either measured locally, or provided by a coordinator. These signals are provided with a time-delay of  $\delta t$ . Smaller the delay  $\delta t$ , less conspicuous would be the affects of the imperfect counteraction of the feed-forward signal. The purpose of the first component of control is to modify the transient characteristics of the response through a control gain K as found by the pole placement techniques. The resulting closed-loop energy dynamics are as follows:

$$\dot{E} = -\left(\frac{R}{2L} + K\right)E + \Delta P^{m}(t) \tag{A.2}$$

Since the control application is a function of the measured power interaction at the interface a sampling timestep  $\delta t$  ahead of time, the closed loop dynamics sees a net disturbance  $\Delta P^m(t)$  Notice that for static power interactions,  $\Delta P^m(t) = 0$  and thus the damping injection does result in current settling down to zero at a closed-loop time constant as modulated by the damping injection gain K.

Now consider the following complex scenarios that are possible in future TeDP systems, the effects of which can be understood through time domain simulations of a representative controllable lossy inductor system in Fig. A.16.

- Non-stationary disturbances: Characteristic of decentralized control actions
   Each Σ<sub>i</sub> designs the control without the knowledge of the neighbor's energy conversion dynamics. As a result, Σ<sub>i</sub> sees zero-mean disturbances, as shown by the red plot in Fig. Appendix A. The effect such disturbance would have on any system with local control, we simulate the trajectories obtained in the simplest case of a representative inductor system in Fig. A.16. The resulting current trajectories are shown in Fig. Appendix A in black. We see that the inductor current trajectory leads to the equilibrium. However, the trajectories would oscillate at the same frequency as that of the disturbance.
- Low inductance: Characteristic of increased power electronics usage

  Present trends of increased power electronic interfacing and decommissioning of diesel engines for greener energy is indicative of the systems with lower inertia. For the same disturbance signal considered in the previous case, if the inductance of the controllable lossy inductor system is made ten times smaller to represent the low inertia systems, the simulated current trajectories are shown in Fig. 17(b) in black. Notice that the magnitude of oscillations increased several folds that it can even trigger the protection devices.
- Non-zero-mean disturbances: Characteristic of challenging mission requirements
   For a persistent dynamic disturbance signal shown in red in Fig. 17(c). The resulting effect on the system is depicted using the lossy inductor example through the resulting time domain simulations of inductor current, as shown in black in Fig. 17(c). Notice for this case that the control design accumulates error over time, and as a result, currents do not ever settle.

Furthermore, consider the same analysis performed using the dual of the system in Fig. A.16. This dual system would be a lossy controllable capacitor where the voltage inputs are replaced with current inputs, and the lossy inductor is replaced with a capacitor with shunt conductance [8]. The voltage trajectories in the dual circuit would be the same as the current oscillations seen

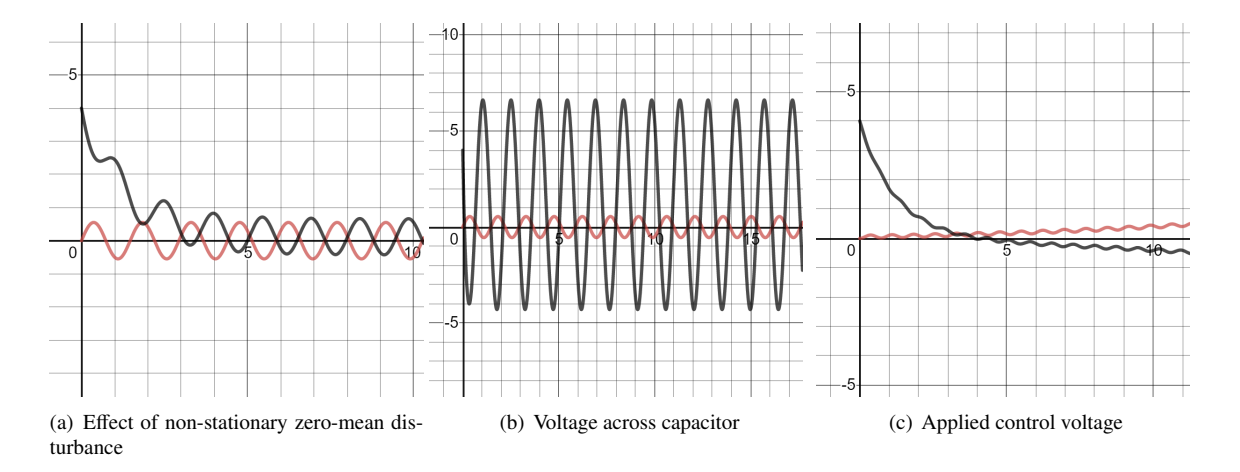


Figure A.17: Current trajectories (in black) obtained for different time-varying disturbances  $\Delta P^{m}(t)$  (in red)

in Fig. A.17. These voltage oscillations are indicative of circulating currents, resulting in increased losses and lower power transfer efficiency.

We have illustrated the detrimental effects changing TeDP systems could have, by performing time domain simulations of a representative simple inductor system. In an actual system, these disturbances could be even worse, because of the parameter and model uncertainty. On the bright side they could be better too. In this analysis of representative inductor system, we have only seen the effect of provable linear quadratic control-based proportional control. However industry today is dominated by PID controllers, where the tuning is performed until the issues with regards to transients or steady-state error are all resolved. However tuning control gains especially for complex systems, suitable for all operating conditions is extremely time-consuming and non-provable.

## Appendix B. Background on physical modeling of electrical machines

In any electrical machine, there are multiple windings carrying current I that are associated with flux linkages  $\psi = LI$  in the air gap. Here, I and  $\psi$  are the vectors associated with respective quantities in each of the windings. L is a symmetric matrix that captures the self and mutual inductances between different windings. The rate of change of flux linkages induces EMF as per Faraday's law of electromagnetism. The flux linkages are often position dependent, which together with the consideration of voltage drop across the resistance of the windings, lead to general form of electrical dynamical

equations in Eqn. (B.1a). Here V is the vector of applied voltages across and R is a diagonal matrix with resistance values of each of the windings.

Furthermore, the current carrying wires in the presence of flux linkages experience a force that is also called as electromagnetic torque  $T_e$  as a result of Lorentz's force law. This phenomena together with Netwon's second law of motion leads to the general form of mechanical dynamical relations in Eqn. (B.1b).

$$\frac{dI}{dt} = L(\theta)^{-1} \left( V - RI - I^{T} \frac{\partial L(\theta)}{\partial \theta} \omega \right)$$
 (B.1a)

$$\frac{d\omega}{dt} = \frac{1}{J} \left( T_m - D\omega - \underbrace{\frac{1}{2} I^T \frac{\partial L(\theta)}{\partial \theta} I}_{T} \right)$$
 (B.1b)

$$\frac{d\theta}{dt} = \omega \tag{B.1c}$$

In the equations above, the components U and  $T_e$  represents the electromechanical coupling. Electric machines used in various architectures differ fundamentally in terms of the construction which dictates the number of winding to be modeled and the position dependence of inductance matrix.

As an example, a synchronous machine consists of three windings on the stator  $(i_a, i_b, i_c)$  and there is a field winding with DC excitation  $(i_f)$  on the rotor that creates electromagnetic flux. In the generation mode, the rotor is driven with an input torque, and the flux linking with the stator windings changes with position of the rotor

thereby inducing and EMF on stator terminals. In the motor mode, the stator terminals are excited with AC voltages carrying AC currents with a phase difference of  $120^0$  creating a rotating magnetic flux in the air gap. The current in the field winding when linked with this magnetic flux experiences an electromagnetic torque. Often other windings called damper windings are modeled on the rotor to capture the effects of eddy currents that flow through the rotor, which are not included here.

In the generator mode, the controls are the field excitation voltage  $v_f$  and input torque  $T_m$ ,  $u = [v_f, T_m]$ . In the motor mode, the control is  $u = [v_f]$ , the mechanical torque enters as a disturbance  $m = [T_m]$ . In both cases, interaction with rest of the system is through the armature terminal voltages applied across each of the phases  $r = [v_a, v_b, v_c]$ . We next utilize the general physics-based structure of machine models to obtain particular machine models in standard state space form.

## Appendix B.1. Example 1: Synchronous machine

Notice that the model in Eqn. (B.1) is a non-linear set of equations, which makes the control problem extremely hard. A trick often utilized in machine modeling is to convert *abc* reference frame quantities into a rotating reference frame with the rotor angle  $\theta$  which is rotating at a speed of  $\omega$  through Park's transformation for balanced three phase quantities as follows [3]. For the case of balanced phases,  $T(\theta)$  operator as defined in Eqn. (B.2) can be used instead to map quantities from and to  $I_{ab} = [i_a, i_b]^T$  and  $I_{dq} = [i_d, i_q]^T$ [3].

$$I_{dq} = \underbrace{\sqrt{2} \left[ \begin{array}{cc} \sin\left(\theta + \frac{\pi}{3}\right) & \sin\left(\theta\right) \\ \cos\left(\theta + \frac{\pi}{3}\right) & \cos\left(\theta\right) \end{array} \right]}_{T(\theta)} I_{ab} \qquad V_{dq} = T(\theta) V_{ab}$$

(B 2)

Upon application of this transformation, the standard state space model can be written as follows:

$$\frac{d}{dt} \begin{bmatrix} i_{d} \\ i_{q} \\ i_{F} \\ \omega \end{bmatrix} = \begin{bmatrix} -\frac{R_{s}}{L_{s,eq}} & 0 & \frac{R_{f}}{M_{eq}} & i_{q} \\ 0 & -\frac{R_{s}}{L_{s,eq}} & 0 & -i_{d} + \frac{M_{eq}}{2L_{s,eq}} i_{f} \\ \frac{R_{s}}{M_{eq}} & 0 & -\frac{R_{f}}{L_{f,eq}} & \frac{M_{eq}}{2L_{f,eq}} i_{q} \\ 0 & -\frac{M_{eq}}{J} i_{f} & 0 & -\frac{D}{J} \end{bmatrix} x$$

$$+ \underbrace{\begin{bmatrix} \frac{1}{L_{s,eq}} & 0 \\ 0 & \frac{1}{L_{s,eq}} \\ 0 & 0 \end{bmatrix}}_{B^{r}} \underbrace{\begin{bmatrix} v_{d} \\ v_{q} \\ v_{q} \end{bmatrix}}_{r} + \underbrace{\begin{bmatrix} 0 & 0 \\ 0 & 0 \\ \frac{1}{L_{f,eq}} & 0 \\ 0 & \frac{1}{J} \end{bmatrix}}_{B^{u}} \underbrace{\begin{bmatrix} v_{F} \\ T_{m} \\ v_{g} \end{bmatrix}}_{u}$$

$$\frac{d\theta}{dt} = \omega$$
(B.3)

Here, the resistances and equivalent self inductances R and  $L_{eq}$  for stator and field windings are identified with subscripts s and f respectively. The mutual inductance is denoted as  $M_{eq}$ . The field excitation and the torque are controllable inputs  $u_i$  while the disturbances enter indirectly through the port inputs  $r_i$ . But for the motor mode of operation,  $v_F$  is controllable input and  $T_m$  is the disturbance.  $r_i$  in some machines is assumed to be controllable through additional power electronics, which will be discussed later. Note that the states of this model are  $x = |i_d, i_q, i_F, \omega, \theta|$ . The coupling between the currents and angular frequency makes this a nonlinear multi-input multi-output control problem. It is typically assumed that the angular frequency evolves much slower than the electromagentic currents. Furthermore, it is assumed that the field current evolves slower than the stator currents. As a result, independent control of the frequency and field current is typically performed by utilizing the resulting linear time-scale separated models [6].

The general standard state space model in linearized form, is shown in Eqn. (B.3). It should be noted that when linearization is performed, matrix A(x) is computed around an equilibrium  $x = x^*$  and thereby converting the problem into **linear multi-input control design problem**.

Appendix B.2. Example 2: Permanent magnet machine

A special case of synchronous machine is the permanent magnetic machine. In this machine, it is assumed that the rotor provides constant magnetization. As a result, this machine is modeled by assuming a fictitious field winding producing a magnetization  $M_{eq}i_F=K$  which is dependent on the rotor position. In Eqn. (B.3), making this substituting and eliminating the dynamics of the fictitious field winding, we obtain the following state space model:

$$\frac{d}{dt} \begin{bmatrix} i_{d} \\ i_{q} \\ \omega \\ \theta \end{bmatrix} = \begin{bmatrix} -\frac{R_{s}}{L_{s,eq}} & 0 & i_{q} & 0 \\ 0 & -\frac{R_{s}}{L_{s,eq}} & -i_{d} + \frac{K}{L_{s,eq}} & 0 \\ 0 & -\frac{K}{J} & -\frac{D}{J} & 0 \\ 0 & 0 & 1 & 0 \end{bmatrix} x + \underbrace{\begin{bmatrix} \frac{1}{L_{s,eq}} & 0 \\ 0 & \frac{1}{L_{s,eq}} \\ 0 & 0 \\ 0 & 0 \end{bmatrix}}_{B^{r}} \underbrace{\begin{bmatrix} v_{d} \\ v_{q} \\ \end{bmatrix}}_{r} + \underbrace{\begin{bmatrix} 0 \\ 0 \\ \frac{1}{J} \\ 0 \end{bmatrix}}_{B^{u}} \underbrace{[T_{m}]}_{u} \tag{B.4}$$

The control design problem posed for this machine as a result can be understood as **non-linear single input** 

**control problem**. The non-linearity is only because of the last column in the matrix A(x) in Eqn. (B.4). Note that these equations are written in rotor reference frame. If they had been written in network reference frame, the corresponding state space model can be written as

$$\frac{d}{dt} \begin{bmatrix} i_d \\ i_q \\ \Delta \omega \\ \delta \end{bmatrix} = \begin{bmatrix} -\frac{R_s}{L_{s,eq}} & \omega_0 & \frac{K \sin(\delta)}{L_{s,eq}} & 0 \\ -\omega_0 & -\frac{R_s}{L_{s,eq}} & \frac{K \cos(\delta)}{L_{s,eq}} & 0 \\ -\frac{K}{J} \sin(\delta) & -\frac{K}{J} \cos(\delta) & -\frac{D}{J} & 0 \\ 0 & 0 & 1 & 0 \end{bmatrix} x \\
+ \underbrace{\begin{bmatrix} \frac{1}{L_{s,eq}} & 0 \\ 0 & \frac{1}{L_{s,eq}} \\ 0 & 0 \end{bmatrix}}_{B^r} \underbrace{\begin{bmatrix} v_d \\ v_q \\ r \end{bmatrix}}_{r} + \underbrace{\begin{bmatrix} 0 \\ 0 \\ \frac{1}{J} \\ 0 \end{bmatrix}}_{B^u} \underbrace{[T_m]}_{u} \tag{B.5}$$

Here the mechanical states or rotor angular position and speed are replaced with relative rotor angle  $\delta$  and relative angular frequency  $\Delta\omega = \omega - \omega_0$ , where  $\omega_0$  is the arbitrary reference frame speed assumed. The control design problem then becomes that of a nonlinear single input control problem. The nonlinearity is a result of trigonometric terms. In the literature, these models often assume small variations of relative angular position and thereby pose the problem as single input linear **control problem**. The single input may not sufficiently be utilized to control the disturbances. As a result, often a rectifier is utilized in conjunction with the PMSG. Furthermore, in the case of motor mode of operation, there is no control at all. In such cases, it becomes imperative to add an inverter in conjunction with the stator windings of the machine.

Appendix B.3. Example 3: Permanent magnet machine with an AC-DC converter

The dynamical model of a typical three-phase AC/DC converter can be written in network reference frame as:

$$\begin{aligned} \frac{di_d}{dt} &= -\frac{R_{PE}}{L_{PE}} i_d + \omega_0 i_q + \frac{1}{L_{PE}} \left( s_d v_{DC} - v_d \right) \\ \frac{di_q}{dt} &= -\frac{R_{PE}}{L_{PE}} i_q - \omega_0 i_d + \frac{1}{L_{PE}} \left( s_q v_{DC} - v_q \right) \\ \frac{dv_{DC}}{dt} &= \frac{1}{C_{PE}} \left( s_d i_d + s_q i_q - i_{DC} \right) \end{aligned}$$
(B.6)

Here,  $R_{PE}$ ,  $L_{PE}$  and  $C_{PE}$  represent the filter impedances and  $i_d$ ,  $i_q$  and  $v_{DC}$  represent the d and q axis equivalent currents of the filter and voltage at the DC interface of the power electronics converter respectively.  $i_{DC}$  is the current entering the DC terminal of the power electronics unit.

We use the same notation for currents here, since two currents flowing into the stator and that into the rectifier unit considered here are the same. Resolving the algebraic dependency, the state space model in standard form for the permagnet machine connected to a rectifier unit can be written as

$$\frac{d}{dt} \begin{bmatrix} i_{d} \\ i_{q} \\ \Delta \omega \\ v_{DC} \end{bmatrix} = \underbrace{\begin{bmatrix} -\frac{R_{s} + R_{PE}}{L_{s,eq} + L_{PE}} & \omega_{0} & \frac{K \sin(\delta)}{L_{s,eq} + L_{PE}} & 0 \\ -\omega_{0} & -\frac{R_{s} + R_{PE}}{L_{s,eq} + L_{PE}} & \frac{K \cos(\delta)}{L_{s,eq} + L_{PE}} & 0 \\ -\frac{K}{J} \sin(\delta) & -\frac{K}{J} \cos(\delta) & -\frac{D}{J} & 0 \\ \frac{s_{d}}{C_{PE}} & \frac{s_{q}}{C_{PE}} & 0 & 0 \end{bmatrix}}_{A(x,u)} x$$

$$+ \underbrace{\begin{bmatrix} 0 \\ 0 \\ \frac{1}{C_{PE}} \end{bmatrix}}_{B^{r}} \underbrace{\begin{bmatrix} i_{DC} \end{bmatrix}}_{r} + \underbrace{\begin{bmatrix} 0 & \frac{v_{DC}}{L_{s,eq} + L_{PE}} & 0 \\ 0 & 0 & \frac{v_{DC}}{L_{s,eq} + L_{PE}} \\ \frac{1}{J} & 0 & 0 \\ 0 & 0 & 0 \end{bmatrix}}_{B^{u}(x)} \underbrace{\begin{bmatrix} T_{m} \\ s_{d} \\ s_{q} \end{bmatrix}}_{u}$$

$$\underbrace{\frac{d\delta}{dt}} = \Delta \omega$$

$$(B.7)$$

Notice that the the port input that enter this module is now the current entering the DC interface. Not only the matrix A is state dependent but is also control dependent. Furthermore, the input matrix is a state dependent matrix. This problem therefore has to be posed as a **bilinear multi-input control problem**. In the state of the art literature, it is typically assumed that the capacitance  $v_{DC}$  is large and thereby under timescale separations assumption, the problem treated as a multi-input linear control problem for small changes in rotor relative angles.

In summary, depending on the objectives of power train, torque control is often sufficient. But other times, when there is a need to control fast disturbances entering the system, switching control is needed. But the resulting control problem is quite complex, But there exists extensive literature of field oriented control originally pursued for induction machines that is now being applied to power electronics converters at the interfaces. The major assumptions involved are that of the small variations of DC voltage and that the field and speed can be independently controlled because of inherent timescale separation of machine models.

## Appendix B.4. Example 4: DC Machine

Finally, we develop the model for DC machine since it is the easiest to study from a control design point of view. The general principles of machine modeling being the same, these machines consists of single winding on the rotor and an external DC source that generates a constant magnetic field. It is assumed in this machine that magnetic field is generated by a field winding which is unaffected by the armature windings. This phenomena is analogous to that of the permanent magnet machine model except that there is a single armature

winding. We can therefore derive DC machine model starting from the permanent magnet machine model in Eqn. (B.3) by using the subscript a instead of q to represent armature quantities and make the d-axis variables equal to zero. The resulting standard state space model is shown in Eqn. (B.8).

$$\frac{d}{dt} \begin{bmatrix} i_{a} \\ i_{F} \\ \omega \end{bmatrix} = \underbrace{\begin{bmatrix} -\frac{R_{a}}{L_{a}} & 0 & k_{B}i_{f} \\ 0 & -\frac{R_{f}}{L_{f}} & 0 \\ -k_{B}i_{f} & 0 & -\frac{D}{J} \end{bmatrix}}_{A(x)} \begin{bmatrix} i_{a} \\ i_{F} \\ \omega \end{bmatrix} + \underbrace{\begin{bmatrix} \frac{1}{L_{a}} \\ 0 \\ 0 \end{bmatrix}}_{B^{r}} + \underbrace{\begin{bmatrix} 0 & 0 \\ 0 & 0 \\ \frac{1}{L_{f}} & 0 \\ 0 & \frac{1}{J} \end{bmatrix}}_{B^{u}} \underbrace{\begin{bmatrix} v_{F} \\ T_{m} \end{bmatrix}}_{u}$$
(B.8)

Here we have denoted  $\frac{M}{L_{eq}}$  with  $k_B$  commonly known as the motor constant. In contrast to the permanent magnet machine model, we model the dynamics of the field winding using the second element on the Eqn. (B.8) under an assumption of negligible magnetic effects that the armature windings would have on the field. With such a model, we can pose the control problem as that of **nonlinear multi-input control design**. Typically, field winding is assumed to evolved much slower, thereby making is a linear control problem. The resulting model is a second order system which can be treated as an equivalent RLC circuit shown in Fig. B.18. With the

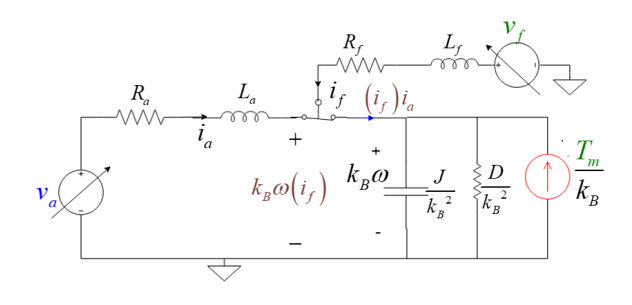


Figure B.18: Equivalent RLC circut of a DC machine: Convention of DC generator is shown here where the control inputs are mechanical torque  $T_m$  and field excitation voltage  $v_F$  labeled in green. The interaction with rest of the system is through the armature voltage  $v_a$  labeled in blue.

field winding modeled however, the equivalent circuit can be understood as if  $i_F$  dynamics dictate the modulation of power from armature to shaft and vice-versa.

## Appendix C. Energy space variables definitions

In what follows, we summarize definitions of energy variables used in the modeling introduced in Section 4.

#### **Definition 2.** (*Instantaneous power*)

The power interaction of the component i with the rest of the system is given by the mapping  $P_i: \mathcal{E}_i \times \mathcal{F}_i \to \mathcal{P}_i$  and is defined as

$$P_i = e_i^T f_i \tag{C.1a}$$

where  $v_i \in \mathcal{E}_i$  and  $f_i \in \mathcal{F}_i$  respectively represent the effort and flow variables appearing at the ports of interconnection.

Based on port variable characterization, we further define generalized rate of reactive power as follows:

**Definition 3.** (Generalized reactive power dynamics) Generalized reactive power  $Q_i$  is a quantity, the time derivative of which is given by a mapping  $\dot{Q}_i : \mathcal{T}\mathcal{E}_i \times \mathcal{TF}_i \to \mathcal{T}Q_i$  and is defined as

$$\dot{Q}_i = e_i^T \frac{df_i}{dt} - f_i^T \frac{de_i}{dt}$$
 (C.1b)

where  $T\mathcal{E}_i$  and  $T\mathcal{F}_i$  represents the tangent manifold of efforts and flow variables respectively.

Let the inertia of the component model in Eqn. (2) be characterized using an inertia matrix  $H_i(x_i)$  [19, 25].

## **Definition 4.** (Stored energy)

Stored energy of component i is given by the energy function  $E_i: X_i \to \mathbb{R}$  defined as

$$E_i(x_i) = \frac{1}{2}x_i^T H_i(x_i)x_i$$
 (C.1c)

for an inertia matrix  $H_i(x_i) \forall x_i \in \mathcal{X}_i$ .

## **Definition 5.** (Stored energy in tangent space)

Given the positive definite inertia matrix  $H_i(x_i)$  used to define stored energy as in Definition 4, the stored energy in tangent space  $E_{ti}$  is defined over the tangent bundle  $\mathcal{T}X_i := \bigcup_{x_i \in X_i} x_i \times T_{x_i} X_i$  where  $T_{x_i} X_i$  is the tangent space of  $X_i$  at  $x_i$ , through the mapping  $E_{t,i} : \mathcal{T}X_i \to \mathbb{R}$  as

$$E_{t,i}(x_i, \dot{x}_i) = \frac{1}{2} \dot{x}_i^T H_i(x_i) \dot{x}_i$$
 (C.1d)

Similar to inertia matrix  $H_i(x_i)$ , let us denote dissipation matrix through  $B_i(x_i)$ , which is a diagonal matrix.

## **Definition 6.** (Time constant)

Dissipation of a component i is described through a

dissipation function in quadratic form through the mapping  $D_i: \mathcal{X}_i \to \mathbb{R}$  defined as

$$D_i(x_i) = x_i^T B_i(x_i)(x_i) x_i$$
 (C.1e)

for some matrix  $B_i(x_i) \forall x_i \in X_i$ . The ratio of stored energy and the damping of the component is called as the time constant.

$$\tau_i = \frac{E_i(x_i)}{D_i(x_i)} \tag{C.1f}$$

From Equations (C.1c) and (C.1e), this quantity can be upper bounded by the largest singular value of  $D_i^{-1}(x_i)H_i(x_i)$ .

## Appendix D. Proof of Theorem 1 of Section 5

*Proof.* (1) Consider now the candidate storage function  $S_i$  as in Eqn. (D.1a).

$$S_{i} = \left( \int_{0}^{t} 4E_{t,i}(s)ds + \frac{1}{\tau_{i}}E_{i}(t) \right) + \left| y_{z,i} - y_{z,i}^{ref} \right|$$
 (D.1a)

By taking its time derivative and plugging in the expressions from Eqn. (5), we have

$$\begin{split} \frac{dS_{i}(t)}{dt} &= \begin{pmatrix} \dot{P}_{i}^{r,out}(t) + \dot{Q}_{i}^{r,out}(t) + \dot{P}_{i}^{m}(t) \\ + \dot{Q}_{i}^{m}(t) + \dot{P}_{i}^{u}(t) + u_{z,i} \end{pmatrix} + \\ sign \begin{pmatrix} y_{z,i}(t) - \\ y_{z,i}^{ref}(t) \end{pmatrix} \begin{pmatrix} -4E_{t,i}(t) + \dot{P}_{i}^{r,out}(t) + \dot{Q}_{i}^{r,out}(t) \\ + u_{z,i} + \dot{Q}_{i}^{m}(t) - \dot{y}_{z,i}^{ref} \end{pmatrix} \end{split}$$
 (D.1b)

$$= \left(\dot{P}_{i}^{u}(t) + \dot{P}_{i}^{m}(t)\right) - \left(\begin{array}{c} \dot{y}_{z,i}^{ref}(t) + \\ 4E_{t,i}(t) \end{array}\right) sign\left(\begin{array}{c} y_{z,i}(t) - \\ y_{z,i}^{ref}(t) \end{array}\right) + \left(1 + sign\left(\begin{array}{c} y_{z,i}(t) \\ -y_{z,i}^{ref}(t) \end{array}\right) \right) \left(\begin{array}{c} \dot{P}_{i}^{r,out}(t) + \dot{Q}_{i}^{r,out}(t) \\ + \dot{Q}_{i}^{m}(t) + u_{z,i} \end{array}\right)$$
(D.1c)

Plugging in the control design in Eqn. (12b) where the expression for  $\eta_i$  is expanded using Eqn. (13b), we obtain the following relation.

$$\begin{split} \frac{dS_{i}(t)}{dt} &= \dot{P}_{i}^{u}(t) + \dot{P}_{i}^{m}(t) - \begin{pmatrix} 4E_{t,i}(t) \\ + \dot{y}_{z,i}^{ref}(t) \end{pmatrix} sign\begin{pmatrix} y_{z,i}(t) \\ -y_{z,i}^{ref}(t) \end{pmatrix} \\ &+ \begin{pmatrix} 1 + sign\begin{pmatrix} y_{z,i}(t) \\ -y_{z,i}^{ref}(t) \end{pmatrix} \end{pmatrix} \\ \begin{pmatrix} \dot{P}_{i}^{r,out}(t) + \dot{Q}_{i}^{r,out}(t) + \dot{Q}_{i}^{m}(t) + \\ -\dot{P}_{i}^{r,out}(t - \delta t) - \dot{Q}_{i}^{r,out}(t - \delta t) \\ -\dot{Q}_{i}^{m}(t - \delta t) + 4E_{t,i}(t - \delta t) \\ + \dot{y}_{z,i}^{ref}(t) - K_{i}\begin{pmatrix} y_{z,i}(t - \delta t) \\ -y_{z,i}^{ref}(t - \delta t) \end{pmatrix} \end{pmatrix} \end{split}$$
(D.1d)

Here, we have utilized the previous timestep values of energy space quantities since the time derivatives of states involved in their computation are unknown at present timestep. By utilizing Taylor's series approximation for simplification of the term  $(y_{z,i}(t-\delta t)-y_{z,i}{}^{ref}(t-\delta t))$   $sign(y_{z,i}(t)-y_{z,i}{}^{ref}(t))$ , we obtain

$$\frac{dS_{i}}{dt} = -K_{i} \begin{vmatrix} y_{z,i}(t - \delta t) - \\ y_{z,i}^{ref}(t - \delta t) \end{vmatrix} + \begin{pmatrix} 4E_{t,i}(t - \delta t) + \dot{P}_{i}^{u}(t) \\ + \dot{P}_{i}^{m}(t) + \dot{y}_{z,i}^{ref}(t) \end{vmatrix} - 4\delta E_{t,i} sign \left( y_{z,i}(t) - y_{z,i}^{ref}(t) \right) + \left( 1 + sign \begin{pmatrix} y_{z,i}(t) \\ -y_{z,i}^{ref}(t) \end{pmatrix} \right) \delta \begin{pmatrix} \dot{P}_{i}^{r,out}(t) + \dot{Q}_{i}^{r,out}(t) \\ + \dot{Q}_{i}^{m}(t) \end{pmatrix} \tag{D.1e}$$

Here,  $\delta(x) = x(t) - x(t - \delta t)$  representing difference between values of quantities between two subsequent timesteps. Next, assuming negligible second order effects of the derivative terms  $\delta(\dot{P}_{i}^{r,out}(t) + \dot{Q}_{i}^{r,out}(t) + \dot{Q}_{i}^{m}(t))$  and  $\delta(E_{t,i})$ , we obtain

$$\frac{dS_{i}}{dt} = -K_{i} \left| y_{z,i}(t - \delta t) - y_{z,i}^{ref}(t - \delta t) \right| 
+ \left( 4E_{t,i}(t - \delta t) + \frac{p_{i}(t)}{\tau_{i}} - \dot{y}_{z,i}(t) + \dot{y}_{z,i}^{ref}(t) \right)$$
(D.1f)

Substituting the output variable derivative expression in closed loop, we finally obtain

$$\frac{dS_{i'}}{dt} = -K_i \left| y_{z,i}(t - \delta t) - y_{z,i}^{ref}(t - \delta t) \right| + \left( 4E_{t,i}(t - \delta t) + K_i \left( y_{z,i}(t - \delta t) - y_{z,i}^{ref}(t - \delta t) \right) \right)$$
(D.1g)

For all operating conditions, a sufficient condition for stability in the sense of Lyapunov is to have the second term of the equation considered to be less than zero. Taking the time integral of the second term condition yields the result stated.

## Appendix E. Proof of Lemma 1 of Section 5

*Proof.* At instantaneous time, the feasibility conditions can also be re-stated as an inequality condition to be satisfied element-by-element as  $z_i^{r,out} \le z_i^{r,in}$  Taking the derivative of the first element of the inequality and the second element of the inequality and adding them up, we obtain

$$\dot{P}_i^{r,out} + \dot{Q}_i^{r,out} \le \dot{P}_i^{r,in} + \dot{Q}_i^{r,in}$$
 (E.1a)

By utilizing the definition of outgoing interaction variable in Eqn. (16),

$$\dot{P}_{i}^{r,out} = \dot{p}_{i} + \frac{d}{dt} \left( \frac{1}{\tau_{i}} E_{i} \right)$$
 (E.1b)

$$\dot{Q}_i^{r,out} = 4E_{t,i} - \dot{p}_i \tag{E.1c}$$

Now combining Eqns. (E.1a) - (E.1c), we have

$$\underbrace{\frac{d}{dt} \left( \int_{0}^{t} 4E_{t,i}(s)ds + \frac{1}{\tau} E_{i}(t) \right)}_{S_{i}(t)} \leq \underbrace{\dot{P}_{i}^{r,in} + \dot{Q}_{i}^{r,in}}_{w_{i}(t)}$$
 (E.1d)

The component model in closed loop is thus dissipative w.r.t the sum of incoming interaction variables as defined in  $w_i(t)$  above.

## Appendix F. Proof of Theorem 2 of Section 5

*Proof.* By adding up the dissipativity conditions in Eqn. (E.1d) for each of the components in the network N,

$$\frac{d}{dt} \left( \sum_{i \in \mathcal{N}} V_{i}(x_{i}) \right) \leq \sum_{i \in \mathcal{N}} \left( \dot{P}_{i}^{r,in} + \dot{Q}_{i}^{r,in} \right) 
\sum_{i \in \mathcal{N}} \left( \dot{P}_{i}^{r,out} + \dot{Q}_{i}^{r,out} \right) \leq \sum_{i \in \mathcal{N}} - \left( \sum_{j \in C_{i}} \left( \dot{P}_{j}^{r,out} + \dot{Q}_{j}^{r,out} \right) \right) 
\mathbf{1}_{|\mathcal{N}| \times 1}^{T} \left( \dot{\mathbf{P}}_{i}^{r,out} + \right) \leq -\mathbf{1}_{|\mathcal{N}| \times 1}^{T} \mathbf{L}_{|\mathcal{N}| \times |\mathcal{N}|} \left( \dot{\mathbf{P}}_{j}^{r,out} \right) 
\mathbf{1}_{|\mathcal{N}| \times 1}^{T} \left( \mathbf{I}_{|\mathcal{N}| \times |\mathcal{N}|} + \mathbf{L}_{|\mathcal{N}| \times |\mathcal{N}|} \right) \left( \dot{\mathbf{P}}_{i}^{r,out} + \dot{\mathbf{Q}}_{i}^{r,out} \right) \leq 0 
\Rightarrow \frac{d}{dt} \left( \mathbf{1}_{|\mathcal{N}| \times 1}^{T} \left( \mathbf{I}_{|\mathcal{N}| \times |\mathcal{N}|} + \mathbf{L}_{|\mathcal{N}| \times |\mathcal{N}|} \right) \mathbf{V} \right) \leq 0$$
(F.1)

Here, **P**, **Q** are the vector forms of the components' real and reactive power. |.| operator here represents the cardinality of the set. **I** and **1** respectively represent the identity matrix and the column vector comprising element 1, with its subscript denoting the order. **L** is an interconnection matrix which is a symmetric matrix. Its element  $L_{ij} = 1$  is the components i and j are connected, and zero if not. Finally, V is the vector representation of potential functions considered at each of the components. Each element of V is positive definite since stored energy is always positive and time constant is assumed positive. We therefore have stability in the sense of Lyapunov.

**Remark 2.** Any physical system however has some resistive losses through parasitic conductance at each of the memory-less junctions, making the right hand side of the the inequality in Eqn. (F.1) strictly negative definite, thereby resulting in asymptotic stability of the timevarying equilibrium  $x^*(t)$  corresponding to the timevarying disturbances entering the system.

## Appendix G. TeDP system parameters

In section 7, we have considered the architecture in Fig. 2 for illustrations. It comprises a permanent magnet generator connected to a permanent magnet motor connected through a wire.

The wire parameters considered are  $R_{TL} = 0.01209$  p.u. and  $L_{TL} = 0.52095$  p.u. on a base value of 100 KVA, 80 KV and 60 Hz.

On the same base values, the motor parameters in context of the model in Eqn. (B.5) with a subscript 2 for the motor are tabulated below:

Variable	Meaning	Value
$L_{s,eq2}$	Synchronous inductance (re-	0.1 p.u.
	actance)	
$K_2$	Speed voltage from rotor flux	1 p.u.
	at nominal speed	
$R_{s2}$	Stator Resistance	0 p.u.
$H_2 = \frac{J_2}{2\omega_b}$	Inertia constant	0 p.u. 3.5 s
$D_2$	Damping coefficient	0 p.u.

The generator parameters for use with model in Eqn. (B.5) are:

Variable	Meaning	Value
$L_{s,eq1}$	Synchronous inductance (re-	0.1 p.u.
	actance)	
$K_1$	Speed voltage from rotor flux	1 p.u.
	at nominal speed	
$R_{s1}$	Stator resistance	0 p.u. 10 s
$H_1 = \frac{J_1}{2\omega_b}$	Inertia constant	10 s
$D_1$	Damping coefficient	0 p.u.

The disturbance entering the system is mechanical load torque on the propulsor motor and is primarily determined by the fan blade pitch and the flight condition of the aircraft. The torque is assumed to vary according to the expression in Eqn. (1) where  $T_{m2,0}$  represents a quasi-static value representing the current blade pitch and flight condition.

#### References

- M. Kh AL-Nussairi, R. Bayindir, S. Padmanaban, L. Mihet-Popa, and P. Siano. Constant power loads (cpl) with microgrids: Problem definition, stability analysis and compensation techniques. *Energies*, 10(10):1656, 2017.
- [2] A. Arntz, O. Atinault, and A. Merlen. Exergy-based formulation for aircraft aeropropulsive performance assessment: theoretical development. AIAA journal, 53(6):1627–1639, 2015.
- [3] Kevin D Bachovchin. Design, modeling, and power electronic control for transient stabilization of power grids using flywheel energy storage systems. Ph. D dissertation, 2015.
- [4] Gerald V Brown, Albert F Kascak, Ben Ebihara, Dexter Johnson, Benjamin Choi, Mark Siebert, and Carl Buccieri. Nasa glenn research center program in high power density motors for aeropropulsion. Technical report, National Aeronautics and Space Administration Cleveland, 2005.

- [5] J. Carroll, A. McDonald, and D. McMillan. Reliability comparison of wind turbines with dfig and pmg drive trains. *IEEE Transactions on Energy Conversion*, 30(2):663–670, 2014.
- [6] J Chow and P Kokotovic. Two-time-scale feedback design of a class of nonlinear systems. *IEEE Transactions on Automatic* Control, 23(3):438–443, 1978.
- [7] M. Cucuzzella, K.C. Kosaraju, and J. Scherpen. Voltage control of dc networks: robustness for unknown zip-loads. arXiv preprint arXiv:1907.09973, 2019.
- [8] Charles A Desoer. Basic circuit theory. McGraw-Hill, 2010.
- [9] Slotine Jean-Jacques E, Li, Weiping, et al. Applied nonlinear control, volume 199. Prentice hall Englewood Cliffs. NJ, 1991.
- [10] Mario Garcia-Sanz. Control co-design: an engineering game changer. Advanced Control for Applications: Engineering and Industrial Systems, 1(1):e18, 2019.
- [11] Mario Garcia-Sanz. Control co-design: an engineering game changer. Advanced Control for Applications: Engineering and Industrial Systems, 1(1):e18, 2019.
- [12] David K Hall, Arthur C Huang, Alejandra Uranga, Edward M Greitzer, Mark Drela, and Sho Sato. Boundary layer ingestion propulsion benefit for transport aircraft. *Journal of Propulsion and Power*, 33(5):1118–1129, 2017.
- [13] M. Ilic and R. Jaddivada. Introducing dymonds-as-a-service (dymaas) for internet of things. In 2019 IEEE High Performance Extreme Computing Conference (HPEC), pages 1–9. IEEE, 2019.
- [14] M. Ilic and R. Jaddivada. Unified value-based feedback, optimization and risk management in complex electric energy systems. *Optimization and Engineering*, pages 1–57, 2020.
- [15] M. Ilić, R. Jaddivada, and X. Miao. Scalable electric power system simulator. In 2018 IEEE PES Innovative Smart Grid Technologies Conference Europe (ISGT-Europe), pages 1–6. IEEE, 2018
- [16] M. Ilic and X. Liu. A simple structural approach to modeling and analysis of the interarea dynamics of the large electric power systems: Part i—linearized models of frequency dynamics. In North American Power Symposium, pages 560–569, 1993.
- [17] Marija D Ilić. From hierarchical to open access electric power systems. *Proceedings of the IEEE*, 95(5):1060–1084, 2007.
- [18] Marija D Ilic and Rupamathi Jaddivada. Fundamental modeling and conditions for realizable and efficient energy systems. In 2018 IEEE Conference on Decision and Control (CDC), pages 5694–5701. IEEE, 2018.
- [19] Marija D Ilić and Rupamathi Jaddivada. Multi-layered interactive energy space modeling for near-optimal electrification of terrestrial, shipboard and aircraft systems. *Annual Reviews in Control*, 45:52–75, 2018.
- [20] Marija D Ilic and Rupamathi Jaddivada. Exergy/energy dynamics-based integrative modeling and control for difficult hybrid aircraft missions. In 2019 AIAA/IEEE Electric Aircraft Technologies Symposium (EATS), pages 1–33. IEEE, 2019.
- [21] Marija D Ilić, Rupamathi Jaddivada, and Xia Miao. Rapid automated assessment of microgrid performance software system (ramps). In 2018 IEEE PES Innovative Smart Grid Technologies Conference Europe (ISGT-Europe), pages 1–6. IEEE, 2018.
- [22] R. Jaddivada and M. Ilic. Multi-layered distributed control of electrical energy systems subject to time-varying interactive disturbances. In 2021 Automatica Submitted for Review. IEEE, 2021
- [23] Rupamathi Jaddivada. A unified modeling for control of reactive power dynamics in electrical energy systems. PhD thesis, Massachusetts Institute of Technology, 2020.
- [24] Ralph Jansen, Cheryl Bowman, Amy Jankovsky, Rodger Dyson, and James Felder. Overview of nasa electrified aircraft propulsion (eap) research for large subsonic transports. In 53rd

- AIAA/SAE/ASEE joint propulsion conference, page 4701, 2017.
- [25] Dimitri Jeltsema and Jacquelien MA Scherpen. Multidomain modeling of nonlinear networks and systems. *IEEE Control Sys*tems Magazine, 29(4):28–59, 2009.
- [26] Dugan Roger C.and Thomas S. Key and Greg J. Ball. Distributed resources standards. *IEEE Industry Applications Mag*azine, 12:27–34, 2006.
- [27] H. Kubota and K. Matsuse. Speed sensorless field-oriented control of induction motor with rotor resistance adaptation. *IEEE Transactions on Industry Applications*, 30(5):1219–1224, 1994.
- [28] New Electricity Transmission Software Solutions (NETSS). Smart Aircraft Power System Simulator (SAPSS) Operation Manual, Version 1.7. NASA Small Business Innovation Research (SBIR), Contract Number 80NSSC19C0239, 2020.
- [29] Vietson Nguyen and John Dhyanchand. An implementation of current-mode control for a series-resonant dc-dc converter. In 1987 2nd IEEE Applied Power Electronics Conference and Exposition, pages 266–273. IEEE, 1987.
- [30] Russell H. Thomas, Guo Yueping, Berton Jeffrey, and Fernandez Hamilton. Aircraft noise reduction technology roadmap toward achieving the nasa 2035 goal. In 23rd AIAA/CEAS aeroacoustics conference, p. 3193, 2017.
- [31] Jan C Willems. The behavioral approach to open and interconnected systems. *IEEE control systems magazine*, 27(6):46–99, 2007.
- [32] JL Wyatt and M Ilić. Time-domain reactive power concepts for nonlinear, nonsinusoidal or nonperiodic networks. In *IEEE international symposium on circuits and systems*, pages 387–390. IEEE, 1990.